Timing Jitter Studies In Modelocked Fiber Lasers

by

Jason William Sickler

Submitted to the Department of Electrical Engineering and Computer Science
in partial fulfillment of the requirements for the degree of

Master of Science in Electrical Engineering

at the

MASSACHUSETTS INSTITUTE OF TECHNOLOGY

June 2003

Author ....
Jason William Sickler
Department of Electrical Engineering and Computer Science
May 23, 2003

Certified by..... .....
Erich P. Ippen
Elihu Thomson Professor of Electrical Engineering, Professor of Physics
Thesis Supervisor

Accepted by..... .....
Arthur C. Smith
Chairman, Department Committee on Graduate Students

Timing Jitter Studies In Modelocked Fiber Lasers

by

Jason William Sickler

Submitted to the Department of Electrical Engineering and Computer Science
on May 23, 2003, in partial fulfillment of the
requirements for the degree of
Master of Science in Electrical Engineering

Abstract

Experimental measurement of the RMS timing jitter in an actively, harmonically modelocked, sigma-configuration fiber laser using optical correlations are presented, along with complete theoretical treatment. These results are compared to the theoretical treatment and experimental results of timing noise spectral density measurements. These measurements were obtained with a residual phase noise demodulation technique. The experimental results for the RMS timing jitter were sufficiently similar and support the theory describing and relating the two measurement techniques.

Experimental results measuring the timing jitter and pulse correlations in a P-APM fiber laser, passively modelocked at 10.378MHz are presented. The timing jitter was measured using a frequency discrimination technique. Attempts to extract pulse correlation values and timing jitter values/bounds are made with inconclusive, limited quantitative success. Opportunity for further optimization and improvement exists and may lead to significantly better quantitative results.

Thesis Supervisor: Erich P. Ippen
Title: Elihu Thomson Professor of Electrical Engineering, Professor of Physics

Acknowledgments

It seems that it took forever to complete this thesis, both the research and the writing... But, here it is! Done, and done.

There are many people to thank for their direct and/or indirect help and support. As these things go, I will inevitably forget someone, so my apologies in advance.

First I would like to thank my advisor, Professor Erich P. Ippen, for his encouragement, patience, and insightful discussions. He seems to have a way of explaining things in very clear, intuitive ways. His sense of humor is fantastic, and his love of skiing is a great bonus - I look forward to many ski trips in the future.

The late Professor Hermann A. Haus was an incredible source of inspiration, enthusiasm, energy, and selflessness. Even though I did not work directly with him, he greatly influenced my growth as a researcher. This place will never be the same without him around.

Of the graduate students, I need to start with Matthew Grein. His knowledge is impressive, his down-to-earth demeanor is comfortable, and his patience is seemingly infinite. I cannot say enough good things about him, cannot give him enough credit for helping me get through this thesis, and hope that I have the pleasure to work with him many times in the future.

Juliet Gopinath has intensity that few match. Were it not for her great sense of humor, she would have tried to kill me by now. I must thank her for all her help in taking data for this thesis, and of course, for accidently turning off my laser after I spent two hours to get it running well. (Yeah, I will never let you live that down.)

Peter Rakich, my officemate (most of the time) is another person with a wonderful sense of humor, which I think happens to be very much like my own. When we aren't joking around, he always has an ear to listen, or a stomach to fill. If it weren't for "Ricky" and Waty, I would have spent many a late night meal with no company. Also, thank you to his huge library of everything. I know my great-grandchildren will be checking books out of the Peter Rakich Library someday...

Hold on!...uh...what's going on? I'm...captain of the...Millenium...Fal-con...Laura

Tiefenbruck, here, my partner in crime was a huge source of sanity during our first two years, and is full of infectious laughter. So here's to pronouncing the alphabet, backwards and forwards, and to two years of the breakfast menu tradition.

Kazi Abedin, or Kazi-san, deserves a big thanks. He is one of the friendliest people I know. He helped me a ton during my early days here. I hope that I have the pleasure of working with him again.

Milos Popovic also deserves thanks, especially for all the work done together on our solid state project. We've had many a lunch together and many an interesting discussion on all manner of topics.

Thanks to Sheila Tandon for the times in solid state, and for all those ab workouts - may there be many more. Thanks to Thomas Schibli, for having a refreshing attitude, for great times skiing and snowboarding, and being "off duty". Thanks to Leaf Jiang for always being willing to explain a concept. Dan Ripin was a great influence coming in to MIT, often with interesting perspectives on things. Thanks to Hideyuki Sotobayashi and Shunichi Matsushita for the Japanese lessons. Thanks to Dr. Yuichi Takushima for the friendly conversation and lunches. Thanks to Pei Lin Hsiung and team M.I.S.C. Thanks to Karen Robinson letting me borrow her bike to get home after the T closed. Thanks to Juhi Chandalia for the ride to Haus's Christmas party. Thanks to Aurea Zare for the chats and refreshers on TQE material. Thanks to Aaron Aguirre and Hanfei Shen for the times early on at MIT as we worked our way through classes. Thanks to Felix Grawert for the best trick I pulled since I arrived in Boston, a reminder of this, now a permanent mark on my thesis. Thanks to all the other graduate students that I have not mentioned here.

Thank you to the Professors at MIT that I have had, including Prof. Fujimoto, Prof. Kong, Prof. Orlando, Prof. Bulovic, and Prof. Ram.

Outside the realm of MIT, indeed overall, the first and foremost thanks goes to Jeff and Sandy Sickler, my parents. Any attempt at a list of reasons would inevitably understate what they have given me. My sister, Alisha Sickler, my better half, is a source of balance and is one of the strongest ties I have to the world outside my (narrow) world of MIT. My extended family also deserves much credit for their care

and support over the years.

A very special thank you goes to Loren Cerami. She is a source of love, beauty, caring, reason... and an immense good that have made my past three years much happier and brighter.

Outside lab are my good Boston friends, some of whom have come and gone, but all of whom have been a source of happiness. My housemates, the 26 and 28 Windsor Rd. people, including Laura Durham for all the times hanging out, Mexican food, movies, and novels, Josh McConnell for his wonderful, random, and sometimes wacky sense of humor and love for competition, Rob Lepome for his tricks, optimization ability, and shells and stars, and Tony Lau for the fantastic smoothies, more shells and stars, and great times hanging out. Thank you to David Rivera, Bob Rudin, Sarah Siracuse, Andy Martin and Kenny Lin. Thanks goes out to the "Tang Group" for the fun times, including Sarah Rodriguez, Yi-Shu, and Club Urbana. Thanks to Tracy Hammond for all the times hanging out, especially during our first year. To all of my Boston friends not named here, thank you.

At home, growing up, the group of guys that had a big hand in who I am deserve much credit: Greg Swithers, Jeff Hourihan, Dana Schneider, Donnie Brooks, Matt Koski, and Dan Harabin. May we have many more times together, with and without the alphabet.

Thanks to the proofreaders of this thesis: Juliet Gopinath, Loren Cerami, Peter Rakich, and of course, Professor Ippen.

Finally, I would like to thank the people at Southside High School in Elmira, NY and the University of Rochester for the academic foundation they have provided me, the Department of Defense NDSEG fellowship for providing my funding for the last two years, Jesse Searls and Poseidon Scientific Instruments for loaning the Poseidon Shoe-Box Oscillator to us, and DARPA for the funding that supported my research.

Contents

List of Figures

List of Tables

Chapter 1

Introduction

1.1 Motivation

Considerable interest in short duration, high repetition rate optical pulse sources exists. Many applications that require sources with these characteristics also require low timing jitter; that is to say low uncertainty in the timing of the output pulses. The timing jitter of pulse sources used in these applications is often a limiting factor, thus understanding and reducing timing jitter in mode-locked lasers is of great practical interest.

One application that requires low timing jitter is high-speed optical telecommunications transmitters. Specifically, timing jitter in high-speed optical telecommunications transmitters can cause pulses to deviate from their timing "slot", leading to bit errors, as well as further problems such as pulse interactions.

High-speed optical sampling units for analog-to-digital conversion (ADC) can also benefit from reduced timing jitter. The current goals in effective bit resolution and sampling frequency are beyond the performance of all-electronic ADC systems. Typical goals in effective bit resolution and sampling frequency are 12+ bits and multi-gigahertz frequencies, respectively [1].

A promising approach is to execute some ADC processes in the optical domain instead of the electrical domain. One can conceive of methods to both optically sample (discretize in time) and optically quantize (discretize in magnitude) a signal.

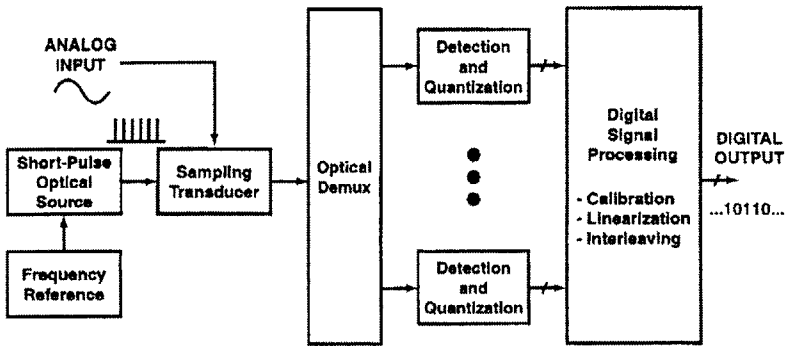

Figure 1-1: Example of an ADC that samples optically and quantizes electronically [1].

We will concentrate on schemes that optically sample and electronically quantize, an example of which is shown in Figure 1-1.

In this diagram, a high-speed, short-pulse, low timing jitter optical source is fed into a sampling transducer, such as an amplitude modulator. The electronic analog input to be sampled drives the transducer, modulating the optical pulse train and thus creating a pulse train where each pulse has sampled the analog signal. Because electronic quantizers are much slower than optical samplers, the sampled signal is demultiplexed into N separate streams, each at a frequency of $\frac{1}{N}$ of the optical sampling frequency. Each of the lower frequency demultiplexed optical streams is then fed to an electronic quantizer. The output of each of the quantizers is then multiplexed and signal processed, resulting in a digital sampling of the analog input.

A recent compilation of the performance of both experimental and commercial ADC systems in terms of effective bit resolution and sampling rate is shown in Figure 1-2. One will notice the constant upper limit in resolution as a function of sampling rate up to around 1 MHz. At sampling rates higher than 1 MHz, the maximum effective bit resolution falls off by around one bit per octave. Analysis shows that the effective bit resolution above 1MHz is limited by aperture jitter [2]. Aperture jitter refers to the fluctuation of the time at which samples are taken. For an optical sampling system, this aperture jitter is synonymous with timing jitter.

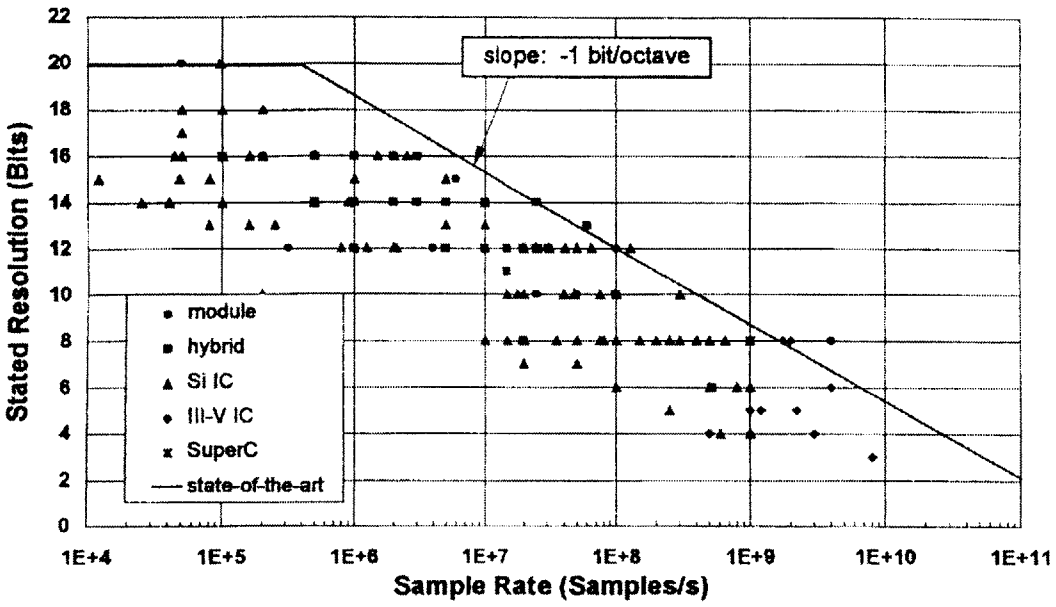

Figure 1-2: Performance survey of current ADC systems [2].

System performance and the limitations timing jitter places on it can be estimated using the following approximation [5]:

$$\sigma < \frac{T}{2^N} \tag{1.1}$$

where T is the repetition rate, N is the effective bit resolution, and sigma is the timing jitter.

Figure 1-3 expresses the same relationship. In this plot, aperture jitter is assumed to be the only noise source. For a given sampling rate and effective bit resolution, one can find a maximum tolerable aperture jitter. The aperture jitter performance for modern electronic and optical sources are shown in the hatched region. One can see that superior ADC performance can be achieved with optical sampling [1].

One should note that the aperture time also effects the performance of these systems. Aperture time refers to the fact that sources put out pulses that are not instantaneous, and thus the values sampled are actually a weighted average of the analog signal over the shape of the sampling pulse. Clearly, shorter, δ function-like pulses are preferable. However, aperture time error is not as significant as aperture

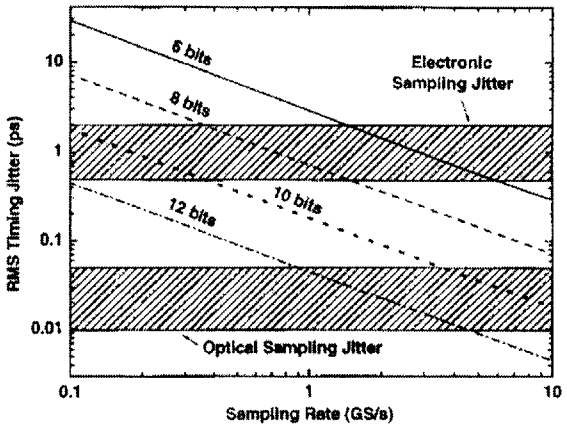

Figure 1-3: Dependence of ADC performance on aperture jitter, when aperture jitter is the only sources of noise. [1]

jitter error, and can be thought of as being included in the aperture jitter [2].

To produce the best optical sampling performance, the ideal optical source should output high frequency pulse trains consisting of short pulses with low timing jitter. Optical sources that hold promise for achieving these goals are semiconductor lasers, solid state lasers., and fiber lasers. This work focuses on efforts on fiber lasers.

To create short pulses in fiber laser systems, fast saturable absorber mechanisms such as polarization additive-pulse modelocking (P-APM) are used. Typically, the fast saturable absorber opens a low-loss window in time, that allow the pulses to build up in this window. The low-loss windows are created by the pulses themselves, using nonlinear effects such as the Kerr effect. Soliton effects further narrow the pulse and limit its duration, while filtering limits the spectrum. The final pulse width reflects the balance of these limiting effects [6].

Generally, high repetition rates can be achieved in two ways. The first is simply to make a short cavity. In this approach, one intracavity pulse exists in the cavity (i.e. the cavity is fundamentally modelocked), and the length of the cavity is reduced, thus increasing the output repetition rate. As an example, to make a 10 GHz laser in a ring configuration, the geometric circumference of the ring will be on the order of 2 mm. This presents problems for many artificial saturable absorber schemes that require

nonlinear effects to accumulate in a roundtrip. Also, fitting the necessary optical components (bandpass filter, waveplates, isolators, etc.) into the cavity becomes difficult.

The second approach is to increase the number of intracavity pulses in the laser; this is known as harmonic modelocking. Harmonic modelocking circumvents many of the problems mentioned above that one encounters in short cavity laser designs, and shows potential for producing low timing jitter pulse trains [4].

1.2 Thesis Organization

This thesis covers two distinct sets of experiments concerned with fiber laser timing jitter. Background for analyzing and understanding the data from these experiments is presented in Chapter 2 through Chapter 4, which covers optical correlations, spectral noise density measurements, and modelocked laser noise. Chapter 5 covers the first set of experiments, which compare and relate two methods of measuring RMS timing jitter. Chapter 6 covers the second set of experiments, where the timing jitter of a 10 MHz passively modelocked P-APM fiber laser is measured using frequency discrimination. Chapter 7 discusses final results, conclusions, and future work. Appendicies follow for reference.

Chapter 2

Optical Correlations and Timing Jitter

This section explores the effect of timing jitter on optical correlation measurements. Results that allow the extraction of the RMS timing jitter using optical correlation measurement results are derived.

2.1 Optical Correlations Involving Timing Jitter

Optical correlations of two pulses are essentially a measure of the convolution of those pulses. Typically, a pulse train is split into two paths, where the length of one path is varied to create a relative delay between the pulse trains. The paths are then crossed, typically inside a nonlinear crystal that generates second harmonic frequencies (SHG)[1]. The intensity of the SHG is proportional to the overlap of the fundamental frequency beam's intensities. The proportionality of the SHG to the intensity of the fundamental frequency can be seen in the semi-classical equation for SHG [8][2]:

[1]There are methods to measure the pulse overlap other than using SHG crystals, including using two-photon absorption in diodes or periodically-poled lithium niobate waveguides [7].

[2]Equation (2.1) is, in general, only one of two coupled equations for sum frequency generation, and is valid for SHG in the undepleted pump approximation. Regardless, an illustration of the intensity dependence of SHG is all that is sought here.

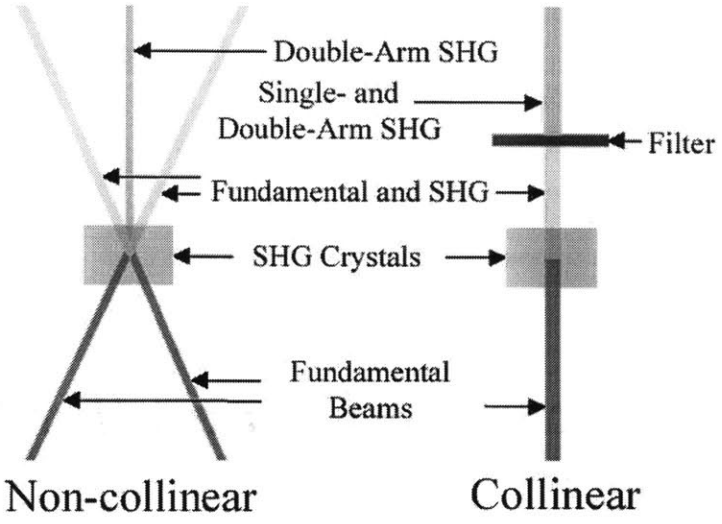

Figure 2-1: Illustration of collinear and non-collinear optical correlator setups. The non-collinear setup allows for easy blocking of the unwanted single-arm SHG. The collinear geometry does not allow for this, but has other advantages, such as the ability to make interferometric optical correlations.

$$\frac{dA_2}{dz} = \frac{4\pi j\omega_2^2 d}{k_2 c^2} A_1^2 e^{i\Delta kz} \tag{2.1}$$

where A_1 is the electric field amplitude of the fundamental frequency, and A_2 is the electric field amplitude of the second harmonic frequency. The second harmonic is measured as a function of the path delay, and the optical correlation trace is created.

All SHG photons originate from two fundamental frequency photons. These SHG photons can be differentiated based on the origin of the fundamental photons from which it came. "Single-arm" SHG is generated from two photons that originated from the same beam. These SHG photons travel in the same direction as the photons from which they originate. "Double-arm" SHG is generated by one photon from each beam. These SHG photons travel in the direction of the average momentum of the two incident photons, and comprise the second harmonic signal that is proportional to the pulse overlap. For non-collinear geometries, where the two incident beam paths do not spatially coincide, the double-arm photons of interest will be spatially separate

from the single-arm photons, and can thus be isolated. This results in a background free optical correlation. Figure 2-1 illustrates this difference between collinear and non-collinear geometries.

The "sliding" overlap integral that will comprise the correlation, will logically look like a convolution function. An expression for the auto-correlation[3] and cross-correlation[4], respectively, where timing jitter is assumed to be absent, can be written:

$$C_{m,m}(t_d) = \int_{-\infty}^{\infty} dt I_m(t) I_m(t + t_d) \tag{2.2}$$

$$C_{m,n}(t_d) = \int_{-\infty}^{\infty} dt I_m(t) I_n(t + t_d) \tag{2.3}$$

where $C_{m,n}(t_d)$ is the expression for the noiseless optical correlation of pulse m and pulse n. $I_m(t)$ is the intensity of pulse m as a function of time, t. t_d represents the time delay between the two pulse streams, modulo the temporal pulse spacing (i.e. the inverse repetition rate).

At this point, noise[5] must be incorporated in the auto-correlation expression. Optical correlation data points are measured on time scales that are much longer than the temporal pulse spacing (i.e. the inverse repetition rate). As such, the optical correlation is the average of the correlation of successive pairs of pulses, where each pulse's nominal timing deviation is random from pair to pair. This suggests that the optical correlation of pulses with timing jitter will be the expectation of the convolution, where now random delays due to timing jitter are included as an argument of the pulse intensity function. Using the basic definition of an expectation, an expression for the optical correlation of two pulses with non-zero timing jitter can be written. For the auto-correlation, this is the expectation of Equation (2.2) with timing noise added:

[3]The auto-correlation is the optical correlation of a pulse with an exact copy of itself.

[4]The cross-correlation is the optical correlation of two pulses in general. The auto-correlation is the special case where the pulses being correlated are identical.

[5]The discussions of noise will require substantial use of probability. A review of probability concepts are included in Section B.1 as a reference for the reader.

$$E[C_{m,m}(t_d, \rho(\Delta T_m, \Delta T_m))] = \int_{-\infty}^{\infty} d\Delta t_m \left[\int_{-\infty}^{\infty} dt I_m(t - \Delta t_m) I_m(t + t_d - \Delta t_m)\right] f_{\Delta T_m}(\Delta t_m) \tag{2.4}$$

where $f_{\Delta T_m}(\Delta t_m)$ is the PDF of the noise ΔT_m, and $\rho(\Delta T_m, \Delta T_n)$ is the correlation coefficient for the random variables ΔT_m and ΔT_n.

Notice that this integral only depends on the relative positions in time of the pulses; any constant time can be added to the argument of both pulses without changing the expression's result. Thus for the optical auto-correlation, since $\rho(\Delta T_m, \Delta T_m) = +1$ always, and assuming the noise variables are identically distributed, Δt_m is added to the argument of each pulse in Equation (2.4):

$$E[C_{m,m}(t_d, \rho(\Delta T_m, \Delta T_m))] = \int_{-\infty}^{\infty} d\Delta t_m \left[\int_{-\infty}^{\infty} dt I_m(t) I_m(t + t_d)\right] f_{\Delta T_m}(\Delta t_m)$$

$$E[C_{m,m}(t_d, \rho(\Delta T_m, \Delta T_m))] = \int_{-\infty}^{\infty} dt I_m(t) I_m(t + t_d) \tag{2.5}$$

Thus the auto-correlation does not change due to the presence of timing jitter.

An expression for the cross-correlation with noise can also be found. The cross-correlation for two pulses, m and n, with timing jitter, results in the general expression for an optical correlation in the presence of timing jitter:

$$\begin{aligned} E[C_{m,n}(t_d, \rho(\Delta T_m, \Delta T_n))] &= \int_{-\infty}^{\infty} d\Delta t_m \int_{-\infty}^{\infty} d\Delta t_n \\ &\left[\int_{-\infty}^{\infty} dt I_m(t - \Delta t_m) I_n(t + t_d - \Delta t_n)\right] f_{\Delta T_m, \Delta T_n}(\Delta t_m, \Delta t_n) \end{aligned} \tag{2.6}$$

where $f_{\Delta T_m, \Delta T_n}(\Delta t_m, \Delta t_n)$ is the joint PDF of ΔT_m and ΔT_n, and the definition of the expectation of functions of two random variables was used.

As a special case, it is seen that if pulse m and n are correlated such that $\rho(\Delta T_m, \Delta T_n) = +1$, and ΔT_m and ΔT_n are identically distributed, then $\Delta T_m = \Delta T_n$. We can therefore add ΔT_m to the argument of both pulses in Equation (2.6):

$$E[C_{m,n}(t_d, \rho(\Delta T_m, \Delta T_n) = +1)] = \int_{-\infty}^{\infty} d\Delta t_m [\int_{-\infty}^{\infty} dt I_n(t) I_m(t + t_d)] f_{\Delta T_m}(\Delta t_m)$$

$$E[C_{m,m}(t_d, \rho(\Delta T_m, \Delta T_n) = +1)] = \int_{-\infty}^{\infty} dt I_m(t) I_m(t + t_d) \tag{2.7}$$

which is equivalent to the cross-correlation without timing jitter, and becomes the expression for the auto-correlation when $m = n$.

Finally, an alternate general expression for Equation (2.6) can be written. Again, nothing is assumed about the timing jitter. By taking advantage once more of the fact that a constant can be added to the argument of both pulses, Δt_m is added to the arguments of both pulses. This results in an alternate general expression for the optical correlation in the presence of timing jitter:

$$E[C_{m,n}(t_d, \rho(\Delta T_m, \Delta T_n))] =$$
$$\int_{-\infty}^{\infty} d\Delta t_m \int_{-\infty}^{\infty} d\Delta t_n [\int_{-\infty}^{\infty} dt I_m(t) I_n(t + t_d + \Delta t_m - \Delta t_n)] f_{\Delta T_m, \Delta T_n}(\Delta t_m, \Delta t_n)$$

$$\boxed{E[C_{m,n}(t_d, \rho(\Delta t_m, \Delta t_n))] = \int_{-\infty}^{\infty} d\Delta t [\int_{-\infty}^{\infty} dt I_m(t) I_n(t + t_d - \Delta t)] f_{\Delta T}(\Delta t)} \tag{2.8}$$

where the definition $\Delta T = \Delta T_n - \Delta T_m$ is made. ΔT is a random variable that describes the difference in the instantaneous timing jitter of the two pulses, and has a PDF, $f_{\Delta T}(\Delta t)$.

Note that Equation (2.6) and Equation (2.8) express the optical correlation for two pulses, where the intensity profile of each pulse and the PDFs of the timing jitter need only be of a well-behaved functional[6] form. Each pulse and each jitter PDF need not be the same, respectively.

[6]By well-behaved, it is meant that the functional forms are such that the interpretations in the derivation are valid. Functions that do not integrate to finite values (i.e. they are not localized) are an example of functions that are not well-behaved. For virtually any real system, these functions will be well-behaved.

2.2 Pulse Width and Timing Jitter Variance Relationships

The integrals in Equation (2.6) or Equation (2.8) can only be done analytically with PDFs and pulse shapes of a very specific form. In general, these equations require numerical calculation. However, results can be derived that will make the numerical work much easier that direct numerical integration. Using analogies with probability, the pulse functions may be treated as PDFs. The pulse widths and optical correlation trace widths may be expressed as the variance width[7]. Finding the variance width will generally require numerical calculation. The calculation results can then be used to calculate the RMS timing jitter using algebraic expressions.

The RMS timing jitter can be easily calculated from the variance width of the timing jitter PDF. The variance width of any function depends on the first and second moment of that function. Only the first and second moments of the functions in the optical correlation expression are needed to calculate the first and second moments of the timing jitter. By working only with these moments, and not the complete functions, the math is simplified considerably.

Beginning with the Equation (2.8) for the general optical correlation of two noisy pulses, $I_m(t)$ and $I_n(t)$ are treated as PDFs. The PDFs must integrate to unity, so the pulse functions are written as follows:

$$I_m(t) = E_m f_m(t) \tag{2.9}$$

where E_m is the pulse energy, and $f_m(t)$ is the pulse shape, normalized so that it's integral is unity.

Now assume $f_m(t)$ is the PDF of a random variable, P_m. The $var(P_m)$, or equivalently, $varW(I_m)$ for the variance width of pulse m, can be found.

This substitution modifies Equation (2.8), as follows:

[7]The variance width, and other related notation, are defined in Section B.2.1

$$E[C_{m,n}(t_d, \rho(\Delta T_m, \Delta T_n))] = E_m E_n \int_{-\infty}^{\infty} d\Delta t \underbrace{\left[\int_{-\infty}^{\infty} dt f_m(t) f_n(t_d - \Delta t + t)\right]} f_{\Delta T}(\Delta t) \tag{2.10}$$

Notice that the integral over t of the two pulse functions resembles a convolution. If $f_m(t)$ is symmetric, the sign of t in $f_m(t)$ can be reversed, the substitution $t \rightarrow -t$ can be made, giving a form that is exactly a convolution.

When the pulse functions are treated as PDFs of P_m and P_n, this convolution results in the PDF of $P_m + P_n = AC$, where AC is a new random variable, and P_m and P_n are independent variables. Thus, the result of this integral is:

$$f_{AC}(t_d - \Delta t) = \int_{-\infty}^{\infty} dt f_m(t) f_n(t_d - \Delta t - t) \tag{2.11}$$

which is just the auto-correlation function. Using the probability rules for sums of independent random variables, the variance width is simply given by:

$$varW(f_{AC}) = varW(I_m) + varW(I_n) \tag{2.12}$$

The equation now reads:

$$E[C_{m,n}(t_d, \rho(\Delta T_m, \Delta T_n))] = E_m E_n \underbrace{\left[\int_{-\infty}^{\infty} d\Delta t f_{AC}(t_d - \Delta t) f_{\Delta T}(\Delta t)\right]} \tag{2.13}$$

This integral is exactly a convolution. This integral will result in the PDF of a new random variable $XC = AC + \Delta T$.

$$f_{XC}(t_d) = \int_{-\infty}^{\infty} dt f_{AC}(t_d - \Delta t) f_{\Delta T}(\Delta t) \tag{2.14}$$

and its variance width is given as

$$varW(f_{XC}) = varW(f_{AC}) + var(\Delta T) \tag{2.15}$$

Now, ΔT is defined as the sum of two random variables, $-\Delta T_m$ and ΔT_n. To remain general, no particular correlation of these variables will be assumed. Using Equation (B.8), the variances of these distributions can be related as follows:

$$varW(\Delta T) = var(\Delta T_n) + var(\Delta T_m) - 2cov(\Delta T_m, \Delta T_n) \tag{2.16}$$

Combining Equation (2.15) and Equation (2.16), the final, general result relating the timing jitter and the auto- and cross-correlation variance widths is found:

$$varW(f_{XC}) = varW(f_{AC}) + var(\Delta T_n) + var(\Delta T_m) - 2\sqrt{var(\Delta T_m)var(\Delta T_n)}\rho(\Delta T_m, \Delta T_n) \tag{2.17}$$

If it is assumed that the timing jitter of each pulse is identically distributed and averages to zero, Equation (2.17) can be solved for the variance of the timing jitter, equivalent to the square of the RMS timing jitter:

$$\boxed{< \Delta T_m^2 >= var(\Delta T_m) = \frac{varW(f_{XC}) - varW(f_{AC})}{2 - \rho(\Delta T_m, \Delta T_n)}} \tag{2.18}$$

Thus, to find the RMS timing jitter from data, only the variance widths of trace data need be taken, the correlation of the pulse noise determined either by measurement or assumption, and the values placed in Equation (2.17) or Equation (2.18), as appropriate.

2.3 Timing Jitter Probability Density Function

The timing jitter that a pulse experiences is the result of many effects, including quantum mechanical noise (vacuum fluctuations and spontaneous emission) added during each pass through the amplifier, thermal noise, and acoustic noise. Often these noise perturbations can be considered independent, and thus, via the Central Limit Theorem, it is reasonable to expect the marginal PDF of the timing jitter of pulse m to be well-approximated by a Gaussian:

$$f_{\Delta T_m}(\Delta t_m) = \frac{1}{\sigma_{\Delta t_m}\sqrt{2\pi}} e^{-\frac{\Delta t_m^2}{2\sigma_{\Delta t_m}^2}} \tag{2.19}$$

where the mean-squared timing jitter equals the variance (i.e. $< \Delta t_m^2 >= \sigma_{\Delta t_m}^2$)[8].

Additionally, the timing jitter can be assumed to be stationary, thus each pulse has the same PDF that is constant in time, the timing jitter PDF can be assumed to be identical from pulse to pulse. As such, $\sigma_{\Delta t_m} = \sigma_{\Delta t_n} = \sigma_{\Delta t}$.

2.4 Timing Jitter Variance for Specific Pulse Forms

Specific functional forms for the pulse shapes will now be explored, and expressions for the RMS timing jitter will be found. All pulses are assumed to be identical - pulse shapes do not vary from pulse to pulse or with time, for times on the order of the time it takes to complete an optical correlation. Relationships between varW and the pulse width parameter, τ, for gaussian and secant hyperbolic pulses are used. These are given in Section B.2.3.

2.4.1 Gaussian Pulses

First, the simplest case of a gaussian pulse shape is considered. For such pulses, one could analytically solve the integrals for the optical correlation functions, and find the RMS timing jitter. However, the general result, Equation (2.18), is used instead.

Consider pulses that are gaussian in shape:

$$I_m(t) = Ae^{-\frac{t^2}{2\tau_p^2}} \tag{2.20}$$

where τ_p is the pulse width parameter.

If the gaussian pulse shape is normalized, and treated like a PDF, the resulting variance width is given as

$$varW(I_m) = \tau_p^2 \tag{2.21}$$

[8]See Section B.1

Using Equation (2.18) and Equation(2.12), the RMS timing jitter is found to be:

$$\Delta T_{RMS} = \sqrt{var(\Delta T_m)} = \sqrt{\frac{varW(f_{XC}) - 2\tau_p^2}{2 - \rho(\Delta T_m, \Delta T_n)}} \tag{2.22}$$

2.4.2 Secant Hyperbolic Pulses

The nonlinear Schrodinger Equation that describes soliton systems has solutions that are secant hyperbolic. As such, it comes as no surprise that the pulses dealt with in soliton fiber lasers are typically secant hyperbolic in shape.

Consider pulses with a secant hyperbolic shape:

$$I_m(t) = Asech\left(\frac{t}{\tau_p}\right) \tag{2.23}$$

where τ_p is the pulse width parameter.

Using the result for the timing jitter in terms of variance widths, Equation (2.18), and the numerical results found in Section B.2.3, the following equation for the RMS timing jitter of two secant hyperbolic pulses is found to be:

$$\Delta T_{RMS} = \sqrt{var(\Delta T_m)} = \sqrt{\frac{varW(f_{XC}) - 4.922\tau_p^2}{2 - \rho(\Delta T_m, \Delta T_n)}} \tag{2.24}$$

These results will be used to calculate the timing jitter from optical correlation data.

2.5 Optical Cross Correlation Delay Line and Dispersion

In practice, when doing an optical cross-correlation, achieving a large range of delays can be difficult. A fiber delay line in one path of the optical correlator is one way to implement this. A nice feature of this approach is the ease with which the delay length may be changed. Group Velocity Dispersion (GVD), however, presents a problem, as the pulses in the delayed optical fiber path will be broadened before they are overlapped with pulses in the other path [4].

The error due to GVD can be calculated and accounted for, assuming higher-order dispersion is negligible. When a dispersive fiber delay is placed in one path of the optical correlator, it will cause pulses in that path to be dispersed when they arrive at the nonlinear crystal. Thus, when the two pulse trains interact in the crystal, one train of pulses will be undispersed and the other will be dispersed. This will change $varW(f_{AC})$, according to Equation (2.12). Thus, the cross-correlation measurement can be corrected given the variance width of the dispersed pulse and the undispersed pulse.

The dispersed and undispersed pulse variance widths can be found by making two auto-correlation measurements, one made with no optical delays anywhere, in order to determine the undispersed pulse width, and one made with the optical delay placed before the pulse train is split into two paths in order to determine the dispersed pulse width. The new expression for the RMS jitter, using a dispersive delay line is then:

$$< \Delta T_m^2 >= var(\Delta T_m) = \frac{varW(f_{XC}) - varW(I_{und}) - varW(I_{disp})}{2 - \rho(\Delta T_m, \Delta T_n)} \tag{2.25}$$

where I_{und} is the pulse shape function for the undispersed pulse, and I_{disp} is the pulse shape function for the dispersed pulse.

2.6 Summary

In this chapter the mathematical treatment of optical correlations including the effects of timing jitter was reviewed. Results relating the pulse width, via the auto- and cross-correlation widths, to the timing jitter variance were derived. The special cases of gaussian and secant hyperbolic pulse shapes were explored. Finally, an expression for the variance of the timing jitter, corrected for the dispersion of a delay line used in cross-correlations, was presented.

Chapter 3

Spectral Noise Density and Timing Jitter

In this chapter I explore the spectral noise density expression for timing jitter, and derive the necessary results for calculating the RMS timing jitter. I then review specific demodulation techniques for measuring the spectral noise density.

3.1 General Derivation of the Spectral Noise Density

The timing jitter of a modelocked laser may be described and understood in the frequency domain. In this section, expressions will be presented for the spectral noise density function for timing jitter. The noise spectral density will be related to the correlation function of the noise of two pulses[1]. This exposition follows [9].

I start by writing the (ensemble) average intensity of an optical pulse train, $\langle I_p(t) \rangle$, as:

[1]For purposes of connecting this Chapter to Chapter 2, one should note that when the expectation of one of the noise variables is zero, the noise correlation function and the covariance are interchangeable. In fact, throughout this work, it will be assumed that the expectation of the noise variables are zero, thus this equivalence holds.

$$\langle I_p(t)\rangle = \sum_m E_p f(t - mT_R) \tag{3.1}$$

where E_p is the average energy of the pulses, $f(t - mT_R)$ is the normalized time-dependent pulse shape, m is an integer indicating the pulse number, and T_R is the inverse repetition rate. Note that I assumed all pulses to have the same shape.

Now, allow the pulse energy and timing to fluctuate from pulse to pulse with random noise variables ΔE_m and ΔT_m, respectively. We can then write an expression for the pulse intensity, expand the resulting expression in a Taylor Series, and keep only first order terms in ΔT_m and $\Delta {E_m}^2$:

$$I(t) = \sum_m (E_p + \Delta E_m) f(t - mT_R - \Delta T_m)$$

$$I(t) = \sum_m (E_p + \Delta E_m) f(t - mT_R) - E_p \sum_m \Delta T_m \frac{d}{dt} f(t - mT_R) + ... \tag{3.2}$$

Assuming that each pulse's timing noise is identically distributed and stationary, $\langle \Delta T_m^2 \rangle$ can be found, given $\langle (\Delta T_0 - \Delta T_m)^2 \rangle$, and $\langle \Delta T_0 \Delta T_m \rangle$, according to Equation (B.8).

Taking the discrete Fourier transform of $\langle \Delta\alpha_0 \Delta\beta_m \rangle$, where variables are generalized to α and β (which can independently be either be T or E), the noise spectral density follows:

$$S_{\Delta\alpha_0,\Delta\beta_m}(\Omega) \equiv \sum_{m=-\infty}^{\infty} \langle \Delta\alpha_0 \Delta\beta_m \rangle e^{-j\Omega m T_R} = \sum_{m=0}^{\infty} 2\langle \Delta\alpha_0 \Delta\beta_m \rangle \cos(-j\Omega m T_R) \tag{3.3}$$

where it is seen that the noise spectral density will alias every $\frac{2\pi}{T_R}$.

To find the $\langle \Delta\alpha_0 \Delta\beta_m \rangle$ in terms of the noise spectral density, the inverse Fourier transform is taken:

$$\langle \Delta\alpha_0 \Delta\beta_m \rangle = T_R \int_{-\pi/T_R}^{\pi/T_R} \frac{d\Omega}{2\pi} S_{\Delta\alpha_0,\Delta\beta_i}(\Omega) e^{j\Omega m T_R} = 2T_R \int_0^{\pi/T_R} \frac{d\Omega}{2\pi} S_{\Delta\alpha_0,\Delta\beta_i}(\Omega) \cos(j\Omega m T_R) \tag{3.4}$$

[2]This effectively neglects distortions in the pulse shape.

where one should note that integral should only be over "one alias" of the spectral noise density.

Using these expressions, the mean-squared timing jitter between two pulses, given the timing jitter spectral density, is:

$$\langle \Delta T^2 \rangle = T_R \int_{-\pi/T_R}^{\pi/T_R} \frac{d\Omega}{2\pi} S_{\Delta T_0, \Delta T_0}(\Omega) \tag{3.5}$$

where the expectation of the timing jitter is taken to be zero. Using this expression, the RMS timing jitter is calculated from the timing jitter spectral density.

3.2 General Demodulation Measurement

Two ways[3] to measure the timing jitter of a modelocked laser are direct detection and demodulation. In direct detection, proposed by von der Linde [11], the laser output intensity is detected. The amplitude noise and timing jitter of the laser output produces noise in the generated photocurrent. This photocurrent is then viewed on an RF signal analyzer, where the amplitude and timing jitter appear as sidebands about the carrier. By looking at several harmonics, one can estimate the timing jitter value, using the fact that sidebands due to timing jitter go as the square of the harmonic number, and the amplitude sidebands are constant. While this method is simple and quick, quantitative results are fairly inaccurate. Much better quantitative results may be obtained using a demodulation technique.

A general demodulation scheme mixes two signals, both of which may contain noise. The mixing products are a baseband set of the noise sidebands with the carrier removed, and a second harmonic signal with noise sidebands. The second harmonic is filtered out, and the baseband noise is observed.

Demodulation has several advantages over direct detection. Direct detection the carrier consumes more of the RF spectrum analyzer's dynamic range, whereas demodulation removes the carrier at baseband, allowing one to view the sidebands using the full dynamic range. Thus one can observe much greater detail in the noise spectrum

[3]Other methods may be used, such as Phase-Encoded Optical Sampling [10].

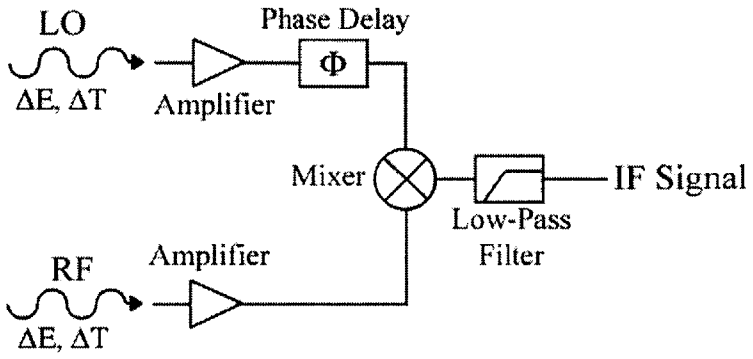

Figure 3-1: Example of a general demodulation scheme for amplitude and timing noise measurement.

and extract more accurate quantitative results. Also, demodulation allows one to bias the measurement system to either suppress amplitude noise or the timing noise, as will be described.

Figure 3-1 illustrates a general demodulation scheme. Two RF signals of the same frequency, both containing amplitude and phase noise, are amplified to appropriate levels, are adjusted in relative phase, and are combined in a mixer. The second harmonic frequency generated by the mixing is filtered with a low-pass filter, and the resulting mixing products are the noise sidebands at baseband.

Note that nothing was said thus far about the origin of the RF signals. The origin of the RF signals is specific to the measurement scheme, and will be covered in Section 3.3.

In this section, the demodulation of two signals with amplitude and timing noise will be derived. Subsequently, two specific demodulation measurements will be examined.

3.2.1 Mixing Products

I begin with the expressions for the time-dependent voltages that are the RF and LO inputs of the mixer. They can be written as:

$$V_{RF}(t) = (V_{RF} + \Delta V_{RF}(t - t_d)) \sin(2\pi f_0(t - t_d) + \Delta\Phi_{RF}(t - t_d)) \tag{3.6}$$

$$V_{LO}(t) = (V_{LO} + \Delta V_{LO}(t)) \cos(2\pi f_0 t + \Delta\Phi_{LO}(t)) \tag{3.7}$$

where V_i are the voltage amplitudes with $i = RF, LO$; f_0 is the nominal frequency of the signals; t_d accounts for any time delay between the RF and LO signals; and $\Delta V_i(t)$ and $\Delta\Phi_i(t)$ are the random variables for the voltage amplitude noise and phase noise, respectively.

Notice that Equation (3.6) and Equation (3.7) are written to be in quadrature when the phase adjustments due to the phase noise variables and delay are the same for both input signals. By mixing the signals in quadrature, the voltage output of the mixers is biased to be most sensitive to phase noise and to suppress the amplitude noise. Figure 3-2 illustrates this. With quadrature biasing, the zero crossing of the LO sinusoid is aligned with the peak of the RF sinusoid. Amplitude fluctuations in the RF signal, being multiplied by the small amplitude of the LO signal in the mixer, are damped out. Phase deviations in the RF sinusoid, however, are multiplied by the peak of the LO signal, resulting in large changes in the mixer output.

To maintain quadrature, it is clear that the time delay in the RF port signal must be discrete such that:

$$t_d = \frac{p_d}{2f_0} \tag{3.8}$$

where $p_d = 0, 1, 2....$ The mixing products of Equation (3.6) and Equation (3.7), after a little algebra, are given as:

$$\begin{aligned}\Delta V(t) = \frac{\alpha}{2}\Big(V_{RF} + \Delta V_{RF}(t - \frac{p_d}{2f_0})\Big)\Big(V_{LO} + \Delta V_{LO}(t)\Big) \\ \Big[\sin\Big(2\pi(2f_0)t - p_d\pi + \Delta\Phi_{RF}(t - \frac{p_d}{2f_0}) + \Delta\Phi_{LO}(t)\Big) \\ + \sin\Big(\Delta\Phi_{RF}(t - \frac{p_d}{2f_0}) - \Delta\Phi_{LO}(t) - p_d\pi\Big)\Big]\end{aligned} \tag{3.9}$$

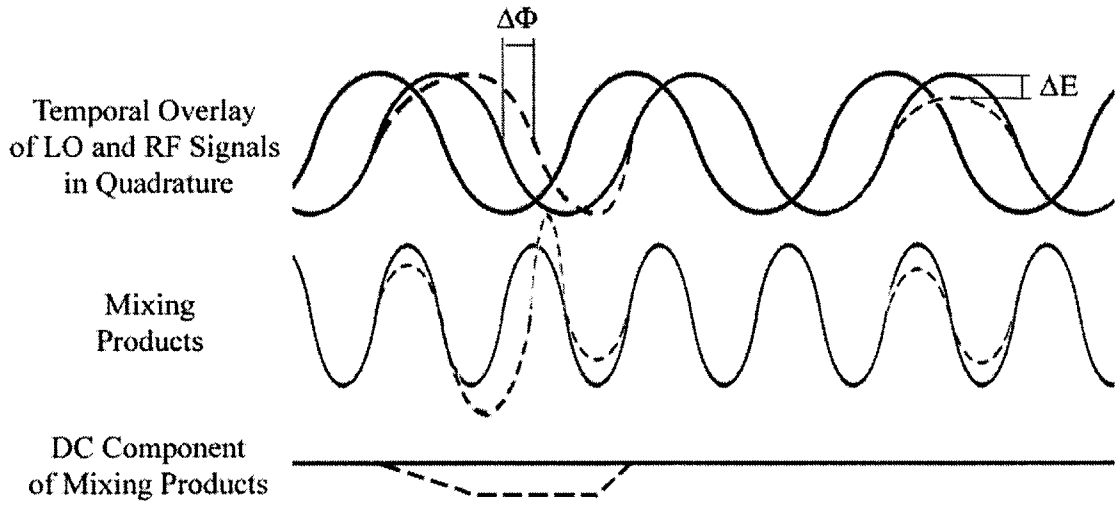

Figure 3-2: An illustration of how quadrature mixing makes the detection system sensitive to phase fluctuations and insensitive to amplitude fluctuations. Fluctuating signals are shown as dashed lines.

where α is the mixing coefficient. The DC and second harmonic results appear clearly. The low-pass filter next strips out the second harmonic component, giving:

$$\begin{aligned}\Delta V(t) &= \pm\frac{\alpha}{2}\Big(V_{RF}V_{LO} + \Delta V_{RF}(t-\frac{p_d}{2f_0})V_{LO} + V_{RF}\Delta V_{LO}(t) + \Delta V_{RF}(t-\frac{p_d}{2f_0})\Delta V_{LO}(t)\Big) \\ &\quad \sin\Big(\Delta\Phi_{RF}(t-\frac{p_d}{2f_0}) - \Delta\Phi_{LO}(t)\Big) \qquad (3.10)\end{aligned}$$

where the sign in front is positive for even p_d and negative for odd p_d.

At this point, all amplitude noise terms are second order or higher. Taking the noise variables to be small, all second and higher order terms are ignored:

$$\Delta V(t) = \pm\frac{\alpha V_{RF}V_{LO}}{2}\sin\left(\Delta\Phi_{RF}(t-\frac{p_d}{2f_0}) - \Delta\Phi_{LO}(t)\right)$$

$$\Delta V(t) = \pm K_\phi \sin\left(\Delta\Phi_{RF}(t-\frac{p_d}{2f_0}) - \Delta\Phi_{LO}(t)\right) \qquad (3.11)$$

where $K_\phi = \frac{\alpha V_{RF}V_{LO}}{2}$.

Assuming that the phase deviations are small compared to a radian, $\Delta\Phi_i << 1$, $\sin(x)$ can be approximated as x, resulting in:

$$\boxed{\Delta V(t) \approx \pm K_\phi \left(\Delta\Phi_{RF}(t - \frac{p_d}{2f_0}) - \Delta\Phi_{LO}(t) \right)} \tag{3.12}$$

Finally, the mean-squared values of Equation (3.12) are found, Equation (3.4) is substituted in, and common integrals and factors are removed, resulting in the phase noise spectral density expression:

$$\boxed{S_{\Delta V,\Delta V}(f_m) = K_\phi^2 \left(S_{\Delta\Phi_{RF},\Delta\Phi_{RF}}(f_m) + S_{\Delta\Phi_{LO},\Delta\Phi_{LO}}(f_m) - 2S_{\Delta\Phi_{RF},\Delta\Phi_{LO}}(f_m)\cos(\Omega m T_R) \right)} \tag{3.13}$$

3.2.2 Phase Noise and Timing Jitter

The phase noise quantities, $\Delta\Phi_i$, can be written in terms of the timing jitter quantities, ΔT_i. This can be simply done using:

$$\Delta\Phi_i(t) = 2\pi f_0 \Delta T_i(t) \tag{3.14}$$

where $i = LO,\ RF$. By taking the mean-squared value of this equation, using Equation (3.4), and removing the common integrals and factors, the timing noise and phase noise spectral densities can be related:

$$S_{\Delta\Phi,\Delta\Phi}(f_m) = (2\pi f_0)^2 S_{\Delta T,\Delta T}(f_m) \tag{3.15}$$

The mixing products can then be cast in terms of the timing noise variables:

$$\Delta V(t) \approx \pm 2\pi f_0 K_\phi \left(\Delta T_{RF}(t - \frac{p_d}{2f_0}) - \Delta T_{LO}(t) \right) \tag{3.16}$$

$$\begin{aligned} S_{\Delta V,\Delta V}(f_m) &= (2\pi f_0 K_\phi)^2 (S_{\Delta T_{RF},\Delta T_{RF}}(f_m) + S_{\Delta T_{LO},\Delta T_{LO}}(f_m) \\ &\quad - 2S_{\Delta T_{RF},\Delta T_{LO}}(f_m)\cos(\Omega m T_R)) \end{aligned} \tag{3.17}$$

3.2.3 Single Sideband Noise and Phase Noise Spectral Density Relationship

The conventional way to express the phase noise of a signal is to display the single sideband (SSB) noise, $\mathcal{L}(f_m)$. This is often taken to be a plot of the noise sidebands that are generated when the carrier is modulated with the noise spectral density, normalized by the total signal power. Assuming that the noise power is small compared to the signal power, $\mathcal{L}(f_m)$ is often approximated as the SSB plot normalized by the carrier power alone. The units of $\mathcal{L}(f_m)$ are dBc/Hz, the power normalized to the carrier power in a 1 Hz bandwidth at f_m offset frequency from the carrier.

For each specific demodulation measurement technique, a relationship between $\mathcal{L}(f_m)$ and the phase noise spectral density, $S_{\Delta\Phi,\Delta\Phi}(f_m)$, is desirable. This relationship will be established. Again, the assumption that the noise power is small compared to the carrier power is used. When a carrier is phase modulated, sidebands are generated, and their magnitudes are Bessel functions of the peak phase deviation of modulation, $J_n(\beta)$, where β is the peak phase deviation. If the phase deviations are taken to be small enough, the Bessel functions can be approximated as β, and the mean-squared phase deviations become $\frac{\beta^2}{2}$. Looking at the ratio of the single sideband power to the carrier power, $\mathcal{L}(f_m)$, $\frac{\beta^2}{4}$ is arrived at, giving:

$$\mathcal{L}(f_m) = \frac{S_{\Delta\Phi,\Delta\Phi}(f_m)}{2} \tag{3.18}$$

This expression can be rewritten in terms of the timing noise spectral density, using Equation(3.14):

$$\mathcal{L}(f_m) = 2(\pi f_o)^2 S_{\Delta T,\Delta T}(f_m) \tag{3.19}$$

The reader is referred to [12] and [13] for more details.

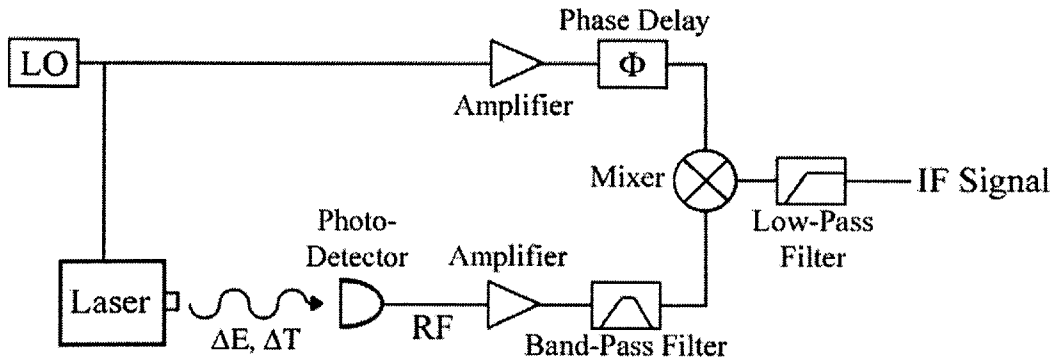

Figure 3-3: A diagram of a residual phase noise setup for laser timing jitter measurement.

3.3 Specific Demodulation Techniques

Using the previous results, two specific demodulation techniques for measuring phase noise will be examined: residual phase noise measurement and frequency discrimination.

3.3.1 Residual Phase Noise Measurement Technique

In this section, the Residual Phase Noise (RPN) demodulation technique for measuring phase noise is outlined. An expression relating the measurement results with the noise spectral density will be derived. This section draws on references [12] and [3].

Figure 3-3 shows a typical RPN setup, and illustrates how the two RF signals analyzed above are derived. The optical pulse train output of the laser is detected, generating a time dependent photocurrent at the fundamental and harmonic repetition rates and of the laser. The harmonic frequencies are filtered out, either by the bandwidth of the detector or explicitly with filters, leaving a single RF frequency at the cavity repetition rate. This signal serves as the RF port input to the mixer:

The signal against which the detected laser output is mixed, the LO port signal, comes from a source where the phase noise as compared to that of the laser pulse train is considered negligible. Typically, for actively modelocked lasers, one derives

the reference signal from the local oscillator that is driving the modelocking element in the laser.

As stated, this technique assumes that the phase noise of the reference signal is negligible, i.e. $\Delta\Phi_{LO} = 0$, compared to that of the laser system under test. In essence, the LO signal is assumed to be a perfect sinusoid. Starting off with Equation (3.11), these assumptions are used, giving:

$$\Delta V(t) \approx K_\phi \Delta\Phi_{RF}(t)$$

The resulting voltage is linearly proportional to the phase deviations created by the timing jitter. Note that $\Delta\Phi(t)$ is a random quantity, and thus $\Delta V(t)$ will also be random. However, for constant phase delays the above equations are still valid, which gives a way to measure K_Φ, as will be seen in Section 6.1.3.

This expression is solved for the phase noise variable, and then rewritten in terms of the timing jitter, using Equation (3.14):

$$\Delta\Phi_{RF}(t) \approx \frac{\Delta V(t)}{K_\phi} \tag{3.20}$$

$$\Delta T_{RF}(t) \approx \frac{\Delta V(t)}{2\pi f_0 K_\phi} \tag{3.21}$$

Using Equation (3.4), the phase noise spectral density, $S_{\Delta\Phi_{RF},\Delta\Phi_{RF}}(f_m)$, can easily be written as a function of the voltage noise spectral density, $S_{\Delta V,\Delta V}(f_m)$. To do this, the mean-squared values of both sides of the Equation (3.20) are taken, are written as integrals of the spectral noise densities, and common integrals are removed:

$$S_{\Delta\Phi_{RF},\Delta\Phi_{RF}}(f_m) \approx \frac{S_{\Delta V,\Delta V}(f_m)}{K_\phi^2} \tag{3.22}$$

which, doing the same for Equation (3.21), the analogous expression for the timing noise spectral density is found:

$$\boxed{S_{\Delta T_{RF},\Delta T_{RF}}(f_m) \approx \frac{S_{\Delta V,\Delta V}(f_m)}{(2\pi f_0 K_\phi)^2}} \tag{3.23}$$

Finally, using Equation (3.18), the single sideband expression for RPN is derived:

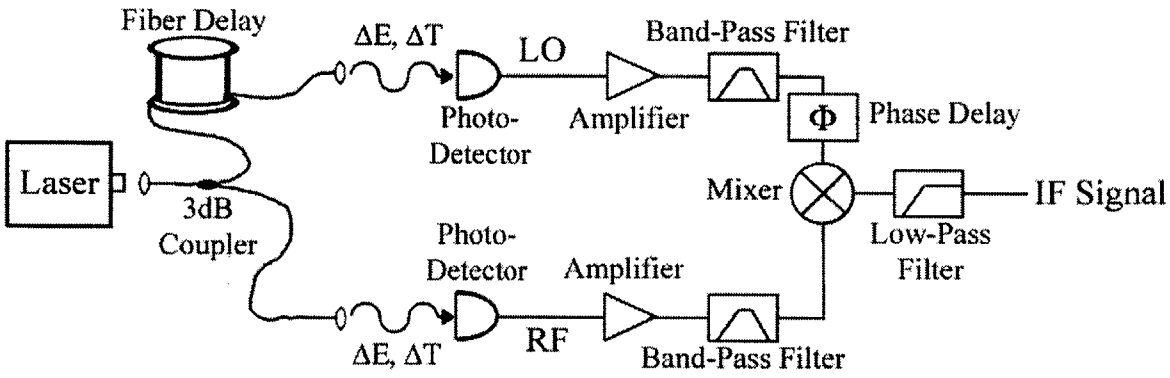

Figure 3-4: A diagram of a frequency discriminator setup to measure laser timing jitter.

$$\boxed{\mathcal{L}_{RPN}(f_m) \approx \frac{S_{\Delta V,\Delta V}(f_m)}{2K_\phi^2}} \tag{3.24}$$

3.3.2 Frequency Discriminator Technique

In this section, the Frequency Discrimination (FD) demodulation technique for measuring phase noise is outlined. An expression relating the measurement results with the noise spectral density will be derived. This section draws on references [12] and [13].

Figure 3-4 shows a typical FD setup, and illustrates the origins of the RF and LO signals. The optical pulse train is split into two essentially identical pulse trains. One pulse train is detected and filtered leaving one harmonic, at frequency f_0 as given in Equation (3.7), of the detected signal - this serves as the LO signal. The other pulse train is delayed by some amount of time, $t_d = \frac{p_d}{2f_0}$, according to Equation (3.8), is then detected, and filtered for one harmonic - this serves as the RF signal. Again, the timing noise of the pulse trains manifest as phase noise in the detected sinusoidal signal, and amplitude fluctuations appear.

The general results of Equation (3.12) and Equation (3.13) are easily specified to this case. The phase noise variables for both the RF and LO signal as a function of time are clearly the same, as they originate from the same pulse train, thus $\Delta\Phi_{RF}(t) =$

$\Delta\Phi_{LO}(t) = \Delta\Phi(t)$. This gives:

$$\Delta V(t) \approx \pm K_\phi \left(\Delta\Phi(t - \frac{p_d}{2f_0}) - \Delta\Phi(t) \right) \tag{3.25}$$

$$S_{\Delta\Phi(t),\Delta\Phi(t)}(f_m) \approx \frac{S_{\Delta V,\Delta V}(f_m)}{2K_\phi^2} + S_{\Delta\Phi(t),\Delta\Phi(t-\frac{p_d}{2f_0})}(f_m) \cos\left(j2\pi f_m \frac{p_d}{2f_0} \right) \tag{3.26}$$

Using Equation (3.14), these two expressions can be written in terms of the timing noise:

$$\Delta V(t) \approx \pm 2\pi f_0 K_\phi \left(\Delta T_{RF}(t - \frac{p_d}{2f_0}) - \Delta T_{LO}(t) \right) \tag{3.27}$$

$$\boxed{S_{\Delta T(t),\Delta T(t)}(f_m) \approx \frac{S_{\Delta V,\Delta V}(f_m)}{2(2\pi f_0 K_\phi)^2} + S_{\Delta T(t),\Delta T(t-\frac{p_d}{2f_0})}(f_m) e^{j2\pi f_m \frac{p_d}{2f_0}}} \tag{3.28}$$

and from these the single sideband measurement is found using Equation (3.18):

$$\boxed{\mathcal{L}(f_m) = \frac{S_{\Delta V,\Delta V}(f_m)}{4K_\phi^2} + 2(\pi f_0)^2 S_{\Delta T(t),\Delta T(t-\frac{p_d}{2f_0})} \cos\left(2\pi f_m \frac{p_d}{2f_0} \right)} \tag{3.29}$$

where the noise spectral densities are for positive frequencies. Notice that the measurement is of $S_{\Delta V}(f_m)$, and an assumption must be made about the correlation of the noise variables.

Sensitivity

The phase modulation of a signal can also be described as a frequency modulation. A signal that undergoes a frequency change will have, after propagating a distance, a resulting phase change as compared to the phase of the signal at the end of the propagation distance before the frequency change occurred. In this way, the delay line converts the frequency deviations associated with the timing jitter into phase deviations proportional to the delay length at the mixer. By analyzing the frequency

discriminator in terms of frequency noise, the frequency discriminator sensitivity can be derived.

The relationship between the phase, timing, and frequency must first be established.

$$\partial f = \frac{1}{2\pi}\frac{\partial \phi}{\partial t} \tag{3.30}$$

The Fourier decomposition of the phase fluctuations can be written and compared to the Fourier decomposition of the frequency fluctuations in order to write the Fourier amplitudes of the phase fluctuations in terms of the Fourier amplitudes of the frequency fluctuations. For a particular frequency of phase modulation, f_m, the phase variable can be written as:

$$\Delta\Phi(t, f_m) = \Delta\Phi_0(f_m)\sin(2\pi f_m t) \tag{3.31}$$

where $\Delta\Phi_0(f_m)$ is the amplitude of the Fourier component of the phase deviations at f_m. Using Equation (3.30), the f_m component of the corresponding frequency modulation, $\Delta F(t, f_m)$, can be found:

$$\Delta F(t, f_m) = \Delta\Phi_0(f_m) f_m \cos(2\pi f_m t) \tag{3.32}$$

Thus, the amplitude of the Fourier component of the frequency modulation, call it $\Delta F_0(f_m)$, is given as:

$$\Delta F_0(f_m) = \Delta\Phi_0(f_m) f_m \tag{3.33}$$

Solving for $\Delta\Phi_0(f_m)$, Equation (3.31) can be substituted:

$$\Delta\Phi(t, f_m) = \frac{\Delta F_0(f_m)}{f_m}\sin(2\pi f_m t) \tag{3.34}$$

Notice that the integrals of Equation (3.31) and Equation (3.32) over (positive) f_m result in the time dependent phase and frequency changes, respectively.

Equation (3.34) is substituted in for the noise variables in Equation (3.25) resulting in the output voltage as a function of time and modulation frequency:

$$\Delta V(t, f_m) \approx \pm K_\phi \left(\frac{\Delta F_0(f_m)}{f_m} \sin(2\pi f_m t - \pi f_m \frac{p_d}{f_0}) - \frac{\Delta F_0(f_m)}{f_m} \sin(2\pi f_m t) \right)$$

$$\Delta V(t, f_m) \approx \pm K_\phi \frac{2\Delta F_0(f_m)}{f_m} \left(\sin(\pi f_m \frac{p_d}{2f_0}) \cos(2\pi f_m t - \pi f_m \frac{p_d}{2f_0}) \right) \tag{3.35}$$

The cosine term describes the time dependent output of the mixer. The coefficient of this cosine, K_{FD}, describes the sensitivity of the system. This coefficient is rewritten as:

$$\boxed{K_{FD} = \pm K_\phi 2\pi \Delta F_0(f_m) \frac{p_d}{2f_0} \frac{\sin(\pi f_m \frac{p_d}{2f_0})}{\pi f_m \frac{p_d}{2f_0}}} \tag{3.36}$$

The sensitivity has a $\frac{sin(x)}{x}$ dependence, with nulls at:

$$f_{m,null} = \frac{1}{t_d} = \frac{2f_0}{p_d} \tag{3.37}$$

Around these nulls, the sensitivity is extremely poor.

Ideally, the frequencies of interest will be well below the first null. A generally accepted criterion is that, if the maximum frequency of interest, f_{max}, is such that:

$$f_{max} < \frac{1}{2\pi t_d} = \frac{f_0}{\pi p_d} \tag{3.38}$$

then the sensitivity can be taken as constant.

For frequencies closer to the null, a correction for the $\frac{sin(x)}{x}$ dependence can be incorporated. However, it must be realized that the sensitivity still degrades closer to the null, and measurements are virtually useless at the null. The generally accepted criterion for valid measurements using a correction for the $\frac{sin(x)}{x}$ dependence is:

$$f_{max} < \frac{1}{2t_d} = \frac{f_0}{p_d} \tag{3.39}$$

Looking back at Equation (3.36), it can be seen that, to improve the sensitivity, the value of the time delay can be increased, via p_d. While this increases the sensitivity,

it decreases the first null frequency, and increasingly limits the range of frequencies at which measurements can be effectively made.

One must also account for, when increasing the delay time, the loss of the delay line. This loss will reduce V_{RF}, and thus reduce K_ϕ. This leads to the existence of an optimal delay length for a particular range of frequencies. For microwave systems, this issue has practical significance. Due to the extremely low loss of optical fiber delay lines, on the order of 0.2 dB/km, however, it is much less of an issue of concern.

Choice of Harmonic Frequency for Phase Detection

One feature of the derived results that should be explored regards the frequency, f_0, that is filtered out and used after the optical pulse train is detected. For a laser system at repetition rate f_{fnd}, the fundamental frequency need not be chosen; any higher harmonic in which there is sufficient power can be used. To account for this possibility, the fundamental frequency is rewritten as:

$$f_0 = N f_{fnd} \tag{3.40}$$

where N is the harmonic number of the harmonic that is chosen.

Unfortunately, it turns out that the change of variables from $\Delta\Phi$ to ΔT brings a factor of $2\pi N f_{fnd}$ according to Equation (3.14), and the relationship between frequency and timing incurs a factor of $\frac{1}{2\pi N f_{fnd}}$ according to Equation (3.30), resulting in the same sensitivity to timing fluctuations. Equation (3.40) is used to rewrite Equation (3.36) as:

$$K_{FD} = \pm K_\phi \pi 2\Delta F_0 \frac{p_d}{2N f_{fnd}} \frac{\sin(\pi f_m \frac{p_d}{2N f_{fnd}})}{\pi f_m \frac{p_d}{2N f_{fnd}}} \tag{3.41}$$

Changing the chosen harmonic, in effect, has the same effect on the sensitivity as changing the delay length.

Changing the harmonic has other implications. In looking at the assumptions made in deriving these results, it is seen that by increasing the operation frequency, the assumption that the phase noise is much less than one radian becomes more

restrictive. Higher harmonics can be used to increase the sensitivity and reduce the need for long delay lines, but only to the extent that the phase noise is still less than one radian at the harmonic frequency.

The Delay Line

The delay line, as shown, has a significant impact on the operation of the frequency discriminator. As such, there are other issues of practical nature regarding the delay line that should be considered and addressed.

The first issues concerns the effect of thermal variations on the delay line. Thermal variation will effect both the physical length of the delay line, and the index of refraction. The latter effect on the index of refraction is much more significant, so physical length variations will be ignored in this discussion.

Typically, the thermal dependence of the index of refraction on temperature is on the order of $n_T \approx 10^{-4}\frac{1}{C^o}$. The time delay of the delay line is given, in terms of refractive index, n, and physical length, L_d, as:

$$t_d = \frac{nL_d}{c} \tag{3.42}$$

where c is the speed of light. Thus, for temperature variation, ΔT, the delay time variation is:

$$\Delta t_d(\Delta T) = \frac{n_T \Delta T L_d}{c} \tag{3.43}$$

These thermal variation will need to be small enough that quadrature is not deviated from significantly.

The thermal time delay variations can be rewritten as thermal phase variations in the detected signal. Using Equation (3.14) of the detected signal, the thermal phase variations are found:

$$\Delta\phi_d(\Delta T) = 2\pi N f_{fnd}\frac{n_T \Delta T L_d}{c} \tag{3.44}$$

As the harmonic frequency of operation is increased, the thermal phase deviation for given temperature change is increased. This means that higher operating frequencies will be more susceptible to thermal variations in the delay line - the delay line becomes more sensitive to both signal variations and thermal variations.

The second question regards the effect that the dispersion in the optical delay line will have on the measurement. Fortunately, the pulse broadening due to dispersion will have no effect on the measurement. The optical pulse train can be written as the sum of Fourier components that comprise the combined RF and optical spectrum of the pulse. Because the detection and filtering only leave a single frequency of the Fourier composition of the pulse train, the dependence of the propagation constant on frequency.

3.4 Summary

In this Chapter, a frequency-domain picture of phase (timing) noise was developed. General demodulation techniques for measuring phase noise were then reviewed. Two specific techniques, residual phase noise and frequency discrimination, were reviewed in detail, sensitivities were derived, and other considerations were discussed.

Chapter 4

Modelocked Laser Noise

4.1 Soliton Theory

In this section, relevant results of soliton theory are briefly summarized. This section follows [14].

The existence of optical soliton solutions in waveguides was first predicted by Hasagawa and Tappert [15]. The Nonlinear Schrodinger Equation is the fundamental equation that governs the formation of solitons, and is given as:

$$j\frac{da}{dz} = \left[-\frac{1}{2}\beta''\frac{d^2}{dt^2} + \eta|a|^2\right]a \tag{4.1}$$

where a is the field, β'' is the group velocity dispersion (GVD)[1], and η is the nonlinear Kerr coefficient. In cases of anomalous dispersion ($\beta'' < 0$), solutions to the NLSE exist, and these are solitons.

The fundamental soliton solution[2] is of the form:

$$a_s(z,t) = \sqrt{P_s}sech\left(\frac{t}{\tau}\right)e^{j\frac{|\beta''|z}{2\tau^2}} \tag{4.2}$$

where τ is the pulse width, and P_s, related to the peak power of the soliton, is given by:

[1] See Section A.1

[2] The fundamental, or N = 1 solution, is the only solution of concern to us, as higher order soliton solutions are unstable.

$$P_s = \frac{|\beta''|}{\eta\tau^2} \tag{4.3}$$

As such, a relationship between the pulse width and peak power, or energy, is set by the system parameters, the dispersion and nonlinear coefficient. This relationship is called the Area Theorem:

$$E_s = 2P_s\tau = \frac{2|\beta''|}{\eta\tau} \tag{4.4}$$

where E_s is the pulse energy.

4.2 The Master Equation

In a soliton laser, effects such as gain, loss, spectral filtering, noise, and active modulation effect the development of the soliton. These effects result in the addition of terms to the NLSE. In addition, the Kerr nonlinearity can, in general, lead to self-phase modulation (SPM) and/or self-amplitude modulation (SAM). Thus, the Kerr nonlinearity term is rewritten where SAM and SPM are separated.

It is also convenient to cast the NLSE in terms of two timescales, t and T. The first time scale, t, is on the order of the pulse duration. The second timescale, T, is on the order of a cavity roundtrip, T_R. Making this change, the NLSE is modified and recast as the Master Equation:

$$T_R\frac{d}{dT}a - \left[jD\frac{\partial^2}{\partial t^2} + (\gamma - j\delta)|a|^2\right]a = \left[g - l + \frac{1}{\Omega_f^2}\frac{\partial^2}{\partial t^2} - \frac{M_{AM} - jM_{PM}}{2}\left(1 - \cos\omega_m t\right)\right]a + T_R S\left(t, T\right) \tag{4.5}$$

where the parameter, D, now expresses the average dispersion in one roundtrip of length d.[3] The Kerr coefficient, η, has been replaced with $\gamma - j\delta$, where γ is the effective SAM coefficient and δ is the effective SPM coefficient. Both are averages

[3]Here, $D = \frac{1}{2}\beta'' d$. This is different than the alternate notation for dispersion, given in Appendix A.1.

over a roundtrip, and thus are proportional to ηd. The spectral filtering is expressed by the filter bandwidth, Ω_f, where the filter shape was Taylor expanded about the peak transmission and includes only terms to second order. The active amplitude and phase modulation depths are expressed by M_{AM} and M_{PM}, respectively, where ω_m is the modulation frequency.[4] Finally, the stochastic variable, $S(t,T)$ drives the noise in the laser. General analytic solutions for this equation have not been found.

One should be careful when comparing the notation here with that of Chapter 3. The driving noise term, $S(t,T)$ is not the representation of the noise spectral densities, $S_{i,j}(f_m)$. Section 4.3.4 provides information that will further clarify the notation.

It is clear that solutions to the Master Equation are not strictly solitons. However, assuming that the effects that were added to the NLSE to arrive at the Master Equation are small per roundtrip, it is reasonable to think that solution to the Master Equation are soliton-like solutions, or solitary pulses.

4.3 Soliton Perturbation Theory

The noise term in Equation (4.5) will be treated in this section. The noise is handled using perturbation theory; as such, the noise perturbation to the NLSE must be assumed small. This section draws on [3][4][16].

4.3.1 Linear Perturbation of NLSE Solution and Equation

One starts by writing our solution as the solution to the NLSE, modified by a small linear perturbation:

$$a(t,T) = [a_s(t) + \Delta a(t,T)]\, e^{-j\frac{\delta}{2}A_0^2\frac{T}{T_R}} \tag{4.6}$$

where $a_s(t,T)$ is the soliton solution to the NLSE using the notation of the Master Equation as given here:

[4]It was assumed that the active amplitude and phase modulation are in phase at the same frequency. Such a situation would occur using a dual-drive amplitude-phase modulator.

$$a_0(t,T) = A_0 sech\left(\frac{t}{\tau}\right) exp\left(-j\frac{\delta}{2}A_0^2\frac{T}{T_R}\right) \tag{4.7}$$

and thus:

$$a_s(t) = A_0 sech\left(\frac{t}{\tau}\right) \tag{4.8}$$

The linearly expanded solution to the NLSE is substituted into the Master Equation, and terms beyond first order in $\Delta a(t,T)$ are ignored. More information on this substitution can be found in [16]. The resulting equation will be used to project out the equations of motion for the pulse parameters.

4.3.2 Expansion of Linear Perturbation in Pulse Parameters

One expands the perturbation, $\Delta a(t,T)$, to first order in a Taylor Series about the exact soliton solution in the four pulse parameters: energy, phase, frequency, and timing:

$$\begin{aligned}\Delta a(t,T) &= \frac{\partial a_s(t)}{\partial w}|_{w=w_0}(w(T)-w_0) + \frac{\partial a_s(t)}{\partial \theta}|_{\theta=\theta_0}(\theta(T)-\theta_0) + \frac{\partial a_s(t)}{\partial p}|_{p=p_0}(p(T)-p_0) \\ &\quad + \frac{\partial a_s(t)}{\partial t}|_{t=t_0}(t(T)-t_0) + a_c(t,T)\end{aligned}$$

$$\Delta a(t,T) = f_w(t)\Delta w(T) + f_\theta(t)\Delta\theta(T) + f_p(t)\Delta p(T) + f_t(t)\Delta t(T) + a_c(t,T) \tag{4.9}$$

where Δi are the noise variables of the respective pulse parameter, and $a_c(t,T)$ is the coupling of the pulse to the continuum.

One can then find the equations of $f_i(t,T)$ functions:

$$f_w(t,T) = \frac{1}{w_0}\left[1 - \frac{t}{\tau}tanh\left(\frac{t}{\tau}\right)\right] a_s(t) \tag{4.10}$$

$$f_\theta(t,T) = j a_s(t) \tag{4.11}$$

$$f_t(t,T) = \frac{1}{\tau}tanh\left(\frac{t}{\tau}\right) a_s(t) \tag{4.12}$$

$$f_p(t,T) = j\frac{2}{w_0}t a_s(t) \tag{4.13}$$

One would like to project a particular noise variable out of the Master Equation to arrive at the equation of motion for that variable. To do this, an orthogonal set of adjoint functions is defined:

$$f_{\_w}(t,T) = 2a_s(t) \tag{4.14}$$

$$f_{\_\theta}(t,T) = 2j\frac{1}{w_0}\left[1-\frac{t}{\tau}tanh\left(\frac{t}{\tau}\right)\right]a_s(t) \tag{4.15}$$

$$f_{\_t}(t,T) = \frac{2}{w_0}ta_s(t) \tag{4.16}$$

$$f_{\_p}(t,T) = j\left(\frac{2}{w_0\tau}tanh\left(\frac{t}{\tau}\right)\right)a_s(t) \tag{4.17}$$

where, by orthogonality:

$$Re\left[\int dt' f^*_{\_i}(t')f_j(t')\right] = \delta_{i,j} \tag{4.18}$$

4.3.3 Projecting Out The Noise Variable Equations of Motion

Equation (4.9) can be substituted into the linearly perturbed Master Equation. The orthogonality of the functions and adjoint functions can then be used to project the pulse parameter noise variables. Doing so leads to the following equations of motion (as a function of T) for the projected noise variables:

$$T_R\frac{\partial}{\partial T}\Delta w = [-2g_s + 2\gamma A_0^2]\Delta w + T_R S_w(T) \tag{4.19}$$

$$T_R\frac{\partial}{\partial T}\Delta\theta = -\delta A_0^2\frac{\Delta w}{w_0} + T_R S_\theta(T) \tag{4.20}$$

$$T_R\frac{\partial}{\partial T}\Delta p = -\frac{4}{3}\frac{g}{\Omega_f^2\tau^2}\Delta p + M_{PM}\omega_m^2\Delta T + T_R S_p(T) \tag{4.21}$$

$$T_R\frac{\partial}{\partial T}\Delta T = -2|D|\Delta p - \frac{\pi^2}{3}\frac{M_{AM}}{2}\omega_m^2\tau^2\Delta T + T_R S_t(T) \tag{4.22}$$

where g_s is the saturated gain, and is defined in terms of other pulse and system parameters. The reader is referred to [16] for details of the manipulation.

In the context of this work, Equation (4.22) and the coupling of the other pulse parameter noise variables is of interest.

4.3.4 Deriving the Noise Spectral Density Equations

Using the equations of motion, the noise spectral density equations in terms of the noise source variables, $S_i(T)$, can be derived. This is most conveniently done in the frequency domain. Thus the following Fourier Transform pair is used:

$$f(\Omega) = \frac{1}{\sqrt{T_0}} \int f(T) e^{-j\Omega T} d\Omega \tag{4.23}$$

$$f(T) = \frac{\sqrt{T_0}}{2\pi} \int f(\Omega) e^{j\Omega T} dT \tag{4.24}$$

where Ω is the angular frequency variable, and the factor of T_0 in front is a normalization time that prevents divergence of the spectrum.

The noise spectral densities in this Chapter will be written as $\langle |\Delta i(\Omega)|^2 \rangle$, where Δi is the noise variable. Given the T_0 factors that appear in the Fourier Transform pairs, $\langle |\Delta i(\Omega)|^2 \rangle$ is the noise spectral density. This change of notation is done to remain consistent with the source literature.

Specific cases can now be observed, and the equations for the timing noise spectral densities can be derived.

4.4 Specific Cases of the Master Equation

The terms that appear in the Master Equation, Equation (4.5), will vary depending on the nature of the system being described. In the following sections active and passive modelocking equations are briefly reviewed, and expressions for the timing noise spectral densities are found.

4.4.1 Active Modelocking

For an actively modelocked soliton laser with amplitude and phase modulation, the Master Equation becomes:

$$T_R\frac{d}{dT}a = \left[jD\frac{\partial^2}{\partial t^2} - j\delta|a|^2\right]a + \left[g - l + \frac{1}{\Omega_f^2}\frac{\partial^2}{\partial t^2} - \frac{M_{AM} - jM_{PM}}{2}\left(1 - \cos\omega_m t\right)\right]a + T_R S\left(t,T\right) \tag{4.25}$$

where the SAM coefficient is set to zero. The resulting equations of motion are:

$$T_R\frac{\partial}{\partial T}\Delta w = -2g_s\Delta w + T_R S_w(T) \tag{4.26}$$

$$T_R\frac{\partial}{\partial T}\Delta\theta = -\delta A_0^2\frac{\Delta w}{w_0} + T_R S_\theta(T) \tag{4.27}$$

$$T_R\frac{\partial}{\partial T}\Delta p = -\frac{4}{3}\frac{g}{\Omega_f^2\tau^2}\Delta p + M_{PM}\omega_m^2\Delta T + T_R S_p(T) \tag{4.28}$$

$$T_R\frac{\partial}{\partial T}\Delta T = -2|D|\Delta p - \frac{\pi^2}{3}\frac{M_{AM}}{2}\omega_m^2\tau^2\Delta T + T_R S_t(T) \tag{4.29}$$

Transforming to the frequency domain, solving for the mean-squared spectrum of the timing noise, and ignoring cross-coupling terms, one finds the expression for the noise spectral density for active modulation:

$$\langle|\Delta T(\Omega)|^2\rangle = \frac{\langle|S_p(\Omega)|^2\rangle\frac{4|D|^2}{T_R^2} + \langle|S_t(\Omega)|^2\rangle\left(\frac{1}{\tau_p^2} + \Omega^2\right)}{\left(\frac{1}{\tau_{AM}^2} + \Omega^2\right)\left(\frac{1}{\tau_p^2} + \Omega^2\right) + \Omega_{PM}^4 + 2\Omega_{PM}^2\left(\frac{1}{\tau_{AM}\tau_p} - \Omega^2\right)} \tag{4.30}$$

where the following parameters are defined as:

$$\Omega_{PM} \equiv \sqrt{2|D|M_{PM}\omega_m^2}\frac{1}{T_R} \tag{4.31}$$

$$\frac{1}{\tau_{AM}} \equiv \frac{\pi^2}{3}\frac{M_{AM}}{2}\omega_m^2\tau^2\frac{1}{T_R} \tag{4.32}$$

$$\frac{1}{\tau_p} \equiv \frac{4}{3\Omega_f^2\tau^2}\frac{1}{T_R} \tag{4.33}$$

Figure 4-1 and Figure 4-2 shows three plots of the phase noise spectrum using realistic values for the equation parameters. One plot is of the phase noise spectrum with pure amplitude modulation ($\Omega_{PM} = 0$) and the other two are with pure phase modulation ($\tau_{AM} \rightarrow \infty$).

4.4.2 Passive Modelocking

In the case of a passively modelocked laser, the Master Equation will take on the following form:

$$T_R \frac{d}{dT} a = \left[jD \frac{\partial^2}{\partial t^2} + (\gamma - j\delta)|a|^2 \right] a + \left[g - l + \frac{1}{\Omega_f^2} \frac{\partial^2}{\partial t^2} \right] a + T_R S(t, T) \tag{4.34}$$

where effective values for γ, and δ will be specific to the passive modelocking mechanism. All active modulation depth parameters have been set to zero. The resulting equations of motion are:

$$T_R \frac{\partial}{\partial T} \Delta w = [-2g_s + 2\gamma A_0^2] \Delta w + T_R S_w(T) \tag{4.35}$$

$$T_R \frac{\partial}{\partial T} \Delta \theta = -\delta A_0^2 \frac{\Delta w}{w_0} + T_R S_\theta(T) \tag{4.36}$$

$$T_R \frac{\partial}{\partial T} \Delta p = -\frac{4}{3} \frac{g}{\Omega_f^2 \tau^2} \Delta p + T_R S_p(T) \tag{4.37}$$

$$T_R \frac{\partial}{\partial T} \Delta T = -2|D| \Delta p + T_R S_t(T) \tag{4.38}$$

Solving for the mean-squared spectrum of the timing noise, and ignoring cross-coupling terms, one finds:

$$\langle |\Delta T(\Omega)|^2 \rangle = \frac{1}{\Omega^2} \left(\frac{4|D|^2}{T_R^2} \frac{\langle |S_p(\Omega)|^2 \rangle}{\frac{1}{\tau_p^2} + \Omega^2} + \langle |S_t(\Omega)|^2 \rangle \right) \tag{4.39}$$

Notice the $\frac{1}{\Omega^2}$ dependence. Because there are no damping terms in the equation of motion for the timing noise, as expected, the timing jitter experiences a random walk.

Figure 4-3 shows a plot of this spectrum in which realistic values for the parameters were used. Experimental analysis in Chapter 6 will make use of Equation (4.39) that generated this plot.

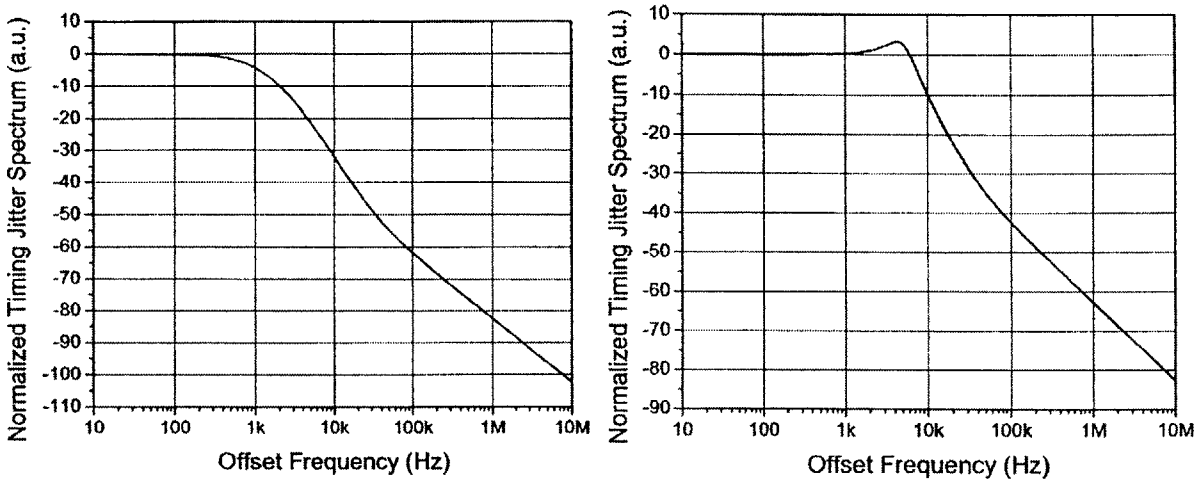

Figure 4-1: Examples of theoretical noise spectral densities for an overdamped (left) and underdamped (right) phase modulation [3].

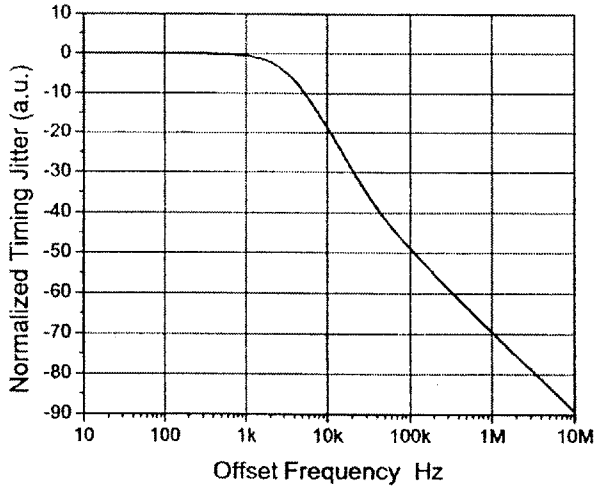

Figure 4-2: Example of the theoretical noise spectral density for amplitude modulation [3].

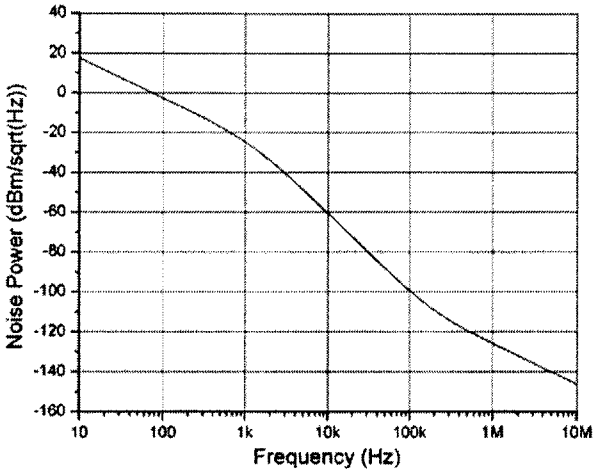

Figure 4-3: Example of the theoretical noise spectral density for passive modelocking.

4.5 Summary

In this chapter, soliton theory was briefly reviewed. The Master Equation and it's solutions were discussed, and perturbation theory was used to treat noise. From this, equations of motion for the mean-squared noise variables were derived. The cases of active and passive modulation were then explored.

Chapter 5

Experiments Comparing Optical Correlation and Spectral Density Timing Jitter Measurements

The first set of experiments performed compares the measurement of the timing jitter of an harmonically modelocked fiber laser using two techniques. One technique uses optical correlations and the fact that the timing jitter effects the cross-correlation width but not the auto-correlation width. The other technique, the residual phase noise technique (RPN), beats in quadrature the detected RF harmonics against a "noiseless" reference signal at the same frequency, and examines the spectrum of the resulting baseband.

5.1 Experimental Setup

I set out to demonstrate experimentally that either a set of optical correlation measurements or a set of noise spectral density measurements would give equivalent results for the RMS timing jitter. This work was done in collaboration with Matthew E. Grein. This section describes the details of the experiments as they were completed.

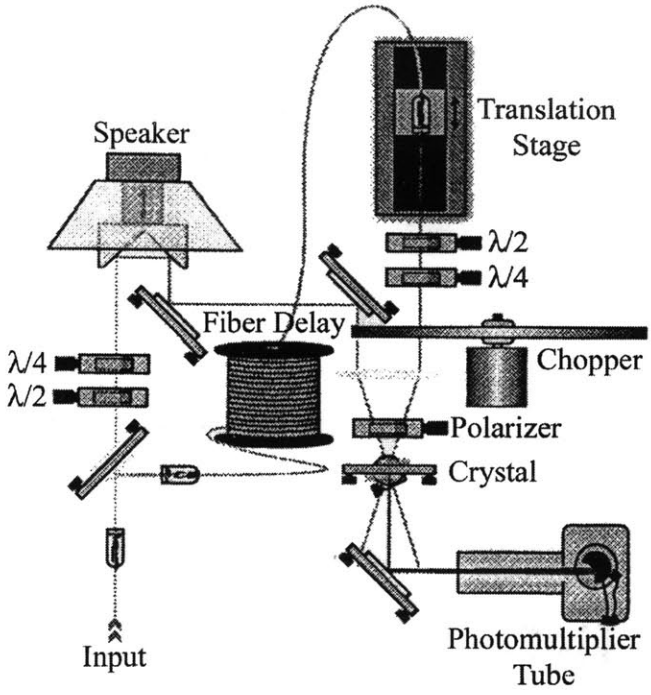

Figure 5-1: Optical Correlator Setup [4].

5.1.1 Optical Correlation Measurement Setup

For the optical correlation measurement, a non-collinear optical correlator with a nonlinear second-harmonic generating POM crystal was used. Figure 5-1 illustrates the design. The delay of one arm is implemented with a motorized translation stage, which is scanned during a correlation. The correlator was built with the option to use a fiber delay to create long delays. In these measurements, the fiber delay was not used. This system was built by Leaf A. Jiang.

5.1.2 Spectral Noise Density Measurement Setup

A residual phase noise measurement system was used to measure the phase noise spectral density. This system is shown in Figure 5-2. The optical pulse train is detected using a Discovery Semiconductor photodiode (Model DSC40S, 16 GHz bandwidth). This signal is amplified with a JSA Technologies Amplifier (Model: JCA812-600,

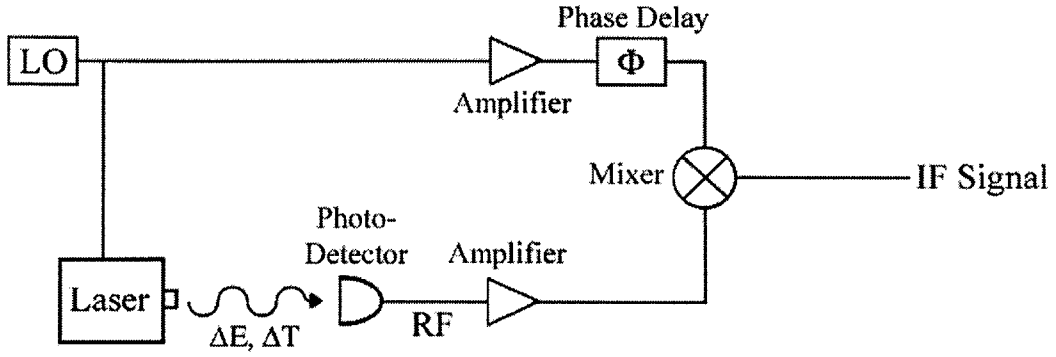

Figure 5-2: Residual Phase Noise Measurement Setup used to measure the timing noise spectral density of the Sigma Laser.

+60dB gain) and beat in quadrature with the output of the Poseidon Shoe-Box Oscillator (9 GHz) that drives the laser modelocker. The DC component of the mixing product is the detected by an Agilent 89410A Vector Signal Analyzer, and the frequency spectral density of this DC voltage is recorded.

5.1.3 Laser System

The laser system (shown in Figure 5-3) used in these experiments is a sigma-configuration actively modelocked fiber laser, built by Matthew E. Grein [3][17]. The ring section of the cavity is made with polarization maintaining components to avoid problems due to polarization rotations caused by random birefringence. The linear section contains an optical filter[1] and a Faraday rotator at the end, so that light propagating in one direction down the linear section returns in the orthogonal polarization. This effectively undoes the random birefringence, which changes on time scales much longer than the round-trip transit times in the linear section. The linear section allows the use of more inexpensive, non-polarization maintaining components.

The round-trip cavity length is 500m. A modulator was used to modelock the laser

[1]Results presented are using a 20nm bandwidth filter. A 10nm bandwidth filter was tried, resulting in greatly reduced timing jitter. Because the aim is to show equivalent timing jitter results for the two measurement techniques, and not show low timing jitter, the 20nm filter was chosen.

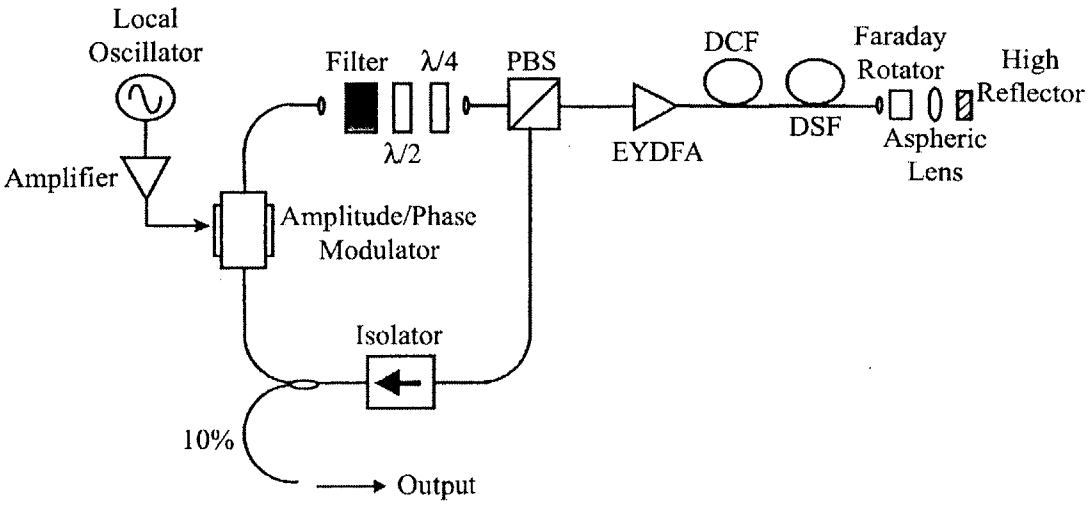

Figure 5-3: Sigma Laser Setup. [3]

at 9GHz. With this length and repetition rate, the harmonic number, the number of intracavity pulses, is calculated to be 22,500.

The modulator was a dual-drive amplitude/phase modulator (Lucent Technologies, Model x2623C, 18GHz bandwidth). This modulator has two RF inputs which allow the $LiNbO_3$ waveguides in each path of the Mach-Zender interferometer to be driven independently, thus allowing both phase and amplitude modulation. Our driving signal, derived from a local oscillator Poseidon Oscillator was split into two paths. An attenuator and phase delay were placed in one path to allow us to modulate the laser as desired.

Because of the long cavity length, thermal drifting of the cavity modes was significant. In order to stabilize the modulation frequency relative to the cavity repetition rate harmonics, a phase-locked loop is used. A piezo cylinder, around which some of the linear section was wrapped, served as the actuator. The feedback from the phase locked loop circuit was then used to stretch the cavity so as to keep its optical length locked to the oscillator. It was found that the modulation could be locked with the cavity length on the order of minutes, and sometimes hours.

The laser output typically consisted of 1.2ps pulses (FWHM), with average power

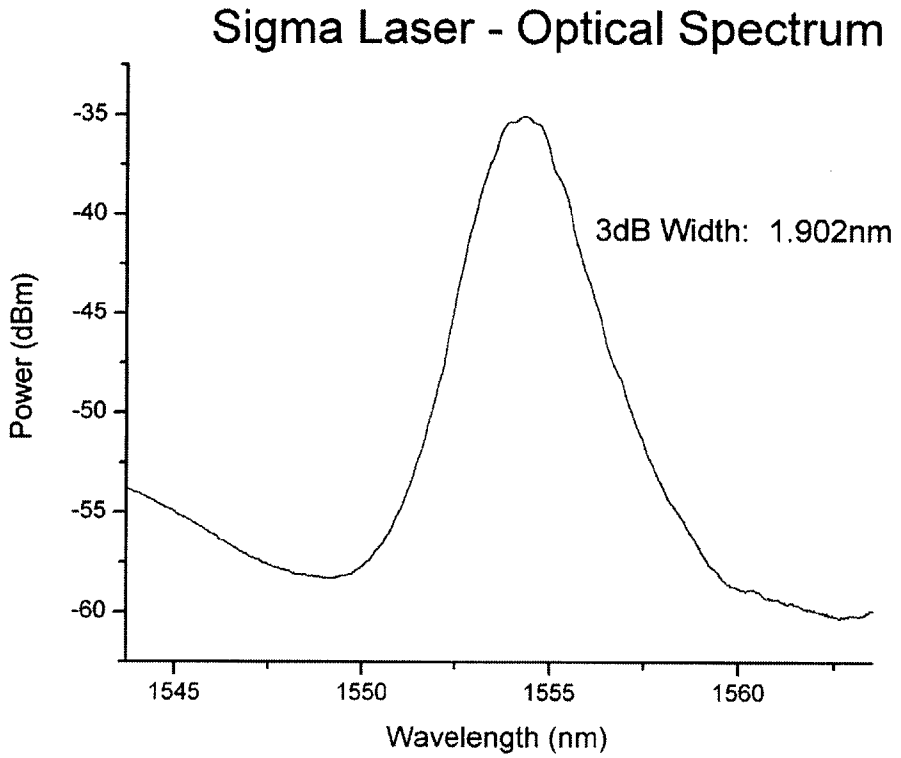

Figure 5-4: Typical optical spectrum of the sigma laser output.

around 7mW. The short pulse duration shows that nonlinear pulse shaping occurs, as such durations would not be achievable otherwise with active modelocking. As such, the pulses are secant hyperbolic.

5.2 Results and Conclusions

The data obtained from the laser diagnostic, optical correlation and noise spectral density measurements will now be examined. From these the RMS timing jitter will be calculated and compared.

Figure 5-4 shows a typical optical spectrum from the laser.

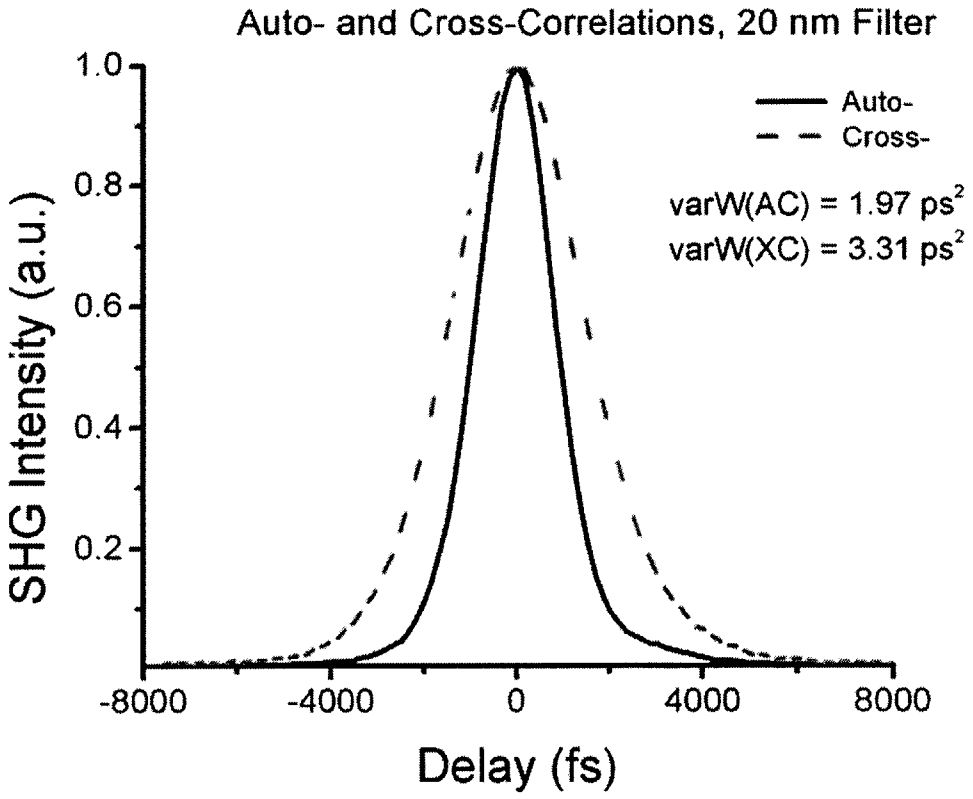

Figure 5-5: Trace of the auto-correlation and cross-correlation of neighboring pulse.

5.2.1 Optical Correlation Measurement Results

The optical auto-correlation and cross-correlations of neighboring pulses are shown in Figure 5-5. The numerically calculated variance widths, using the data that generated these traces, are found to be $varW(XC) = 3.31ps^2$ and $varW(AC) = 1.97ps^2$.

When calculating the timing jitter, it is assumed that neighboring pulses are uncorrelated. Given that the output pulses originate from different intracavity pulses, this assumption is expected to be valid.

Using Equation (2.18) and assuming that the pulses are uncorrelated, an RMS timing jitter calculation results in 819fs. To place conservative bounds on the calculated timing jitter, a $\rho(\Delta T_i, \Delta T_j) = +1$ correlation assumption results in an RMS timing jitter of 1158fs, and a $\rho(\Delta T_i, \Delta T_j) = -1$ correlation assumption results in

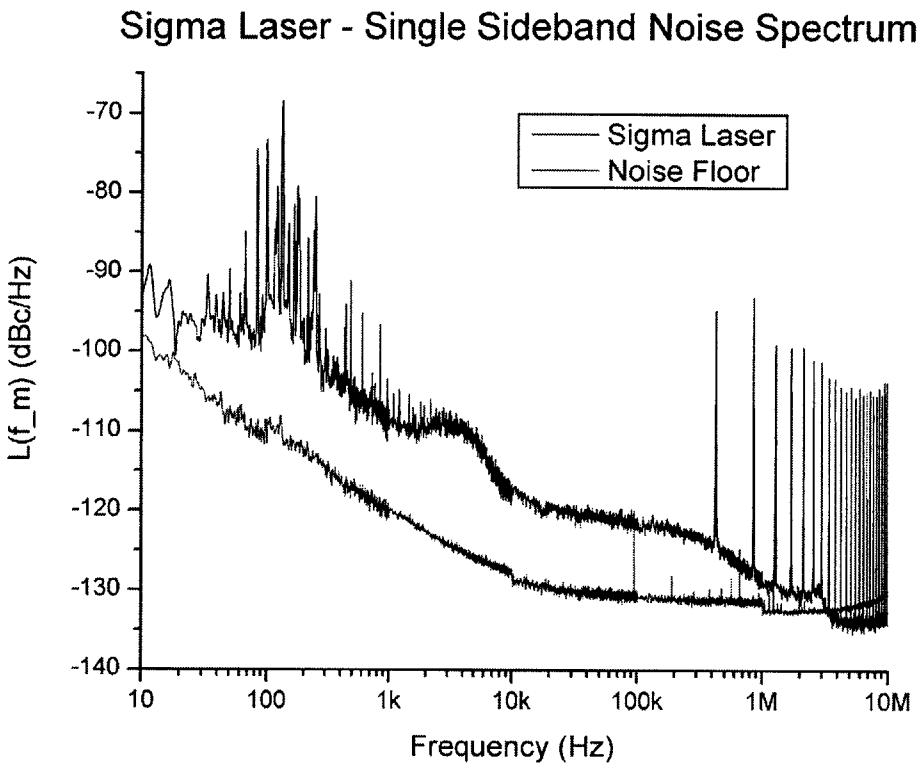

Figure 5-6: Single Sideband measurement of the phase noise spectral density of the sigma laser.

668fs.

5.2.2 Residual Phase Noise Measurement Results

The Residual Phase Noise Measurement trace for the sigma laser is shown in Figure 5-6. The noise floor is plotted to show that the measurement is of noise from the laser and not the measurement device.

From Section 3.1, one must integrate from 0 to $\frac{\pi}{T_R}$ to calculate the mean-squared value of the timing jitter. For the sigma laser, this corresponds to integrating out to $\frac{\pi}{T_R}$, or 4.5GHz, the Nyquist frequency. Unfortunately, the SSB data only extends to 10MHz.

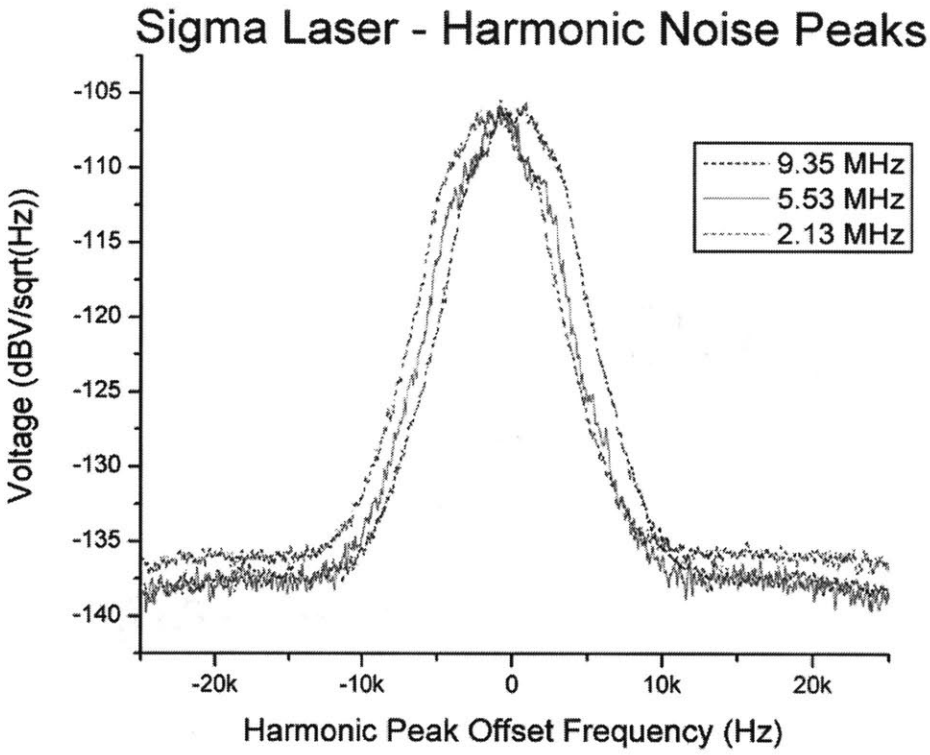

Figure 5-7: An overlay of three noise harmonics taken using an Agilent 8565EC RF Spectrum Analyzer (9kHz - 50GHz). The plots have been offset slightly, to allow for better viewing. They are ordered lowest to highest harmonic, left to right. As expected, the noise harmonics alias.

If it is assumed that the timing jitter of each pulse is identically distributed and uncorrelated, as was done with the optical correlations in Section 5.2.1, then the harmonic noise peaks will alias [9]. Figure 5-7 shows an overlay of the specified harmonic noise peaks, and supports the aliasing claim. Using this assumption, the timing jitter can be calculated by integrating out to 10MHz and multiplying the result by 450 to account for the remaining noise peaks out to the Nyquist frequency. Using this process, an RMS timing jitter of 2619fs is calculated.

5.2.3 Conclusions

The results from each type of measurement are roughly on the same order. A number of factors are likely to have contributed to the disparity.

The optical correlation measurement is limited in its resolution. For many systems with low jitter, including the sigma laser using a 10nm bandwidth optical filter (data not presented), the fractional width change in the cross-correlation is rather small. This can make it difficult to resolve, and lead to error.

In the residual phase noise measurement, the assumption that the oscillator timing noise and the laser output noise are uncorrelated may not be accurate. The laser modelocker is driven by the oscillator, and thus the laser and modelocking oscillator cannot be totally independent. The assumption that the noise contribution of the local oscillator is zero is also not exact. It is expected that this source of error, however, is not very large, considering the specifications of the Poseidon oscillator (-112 dBc/Hz @ 100Hz, -141 dBc/Hz @ 1kHz, -161 dBc/Hz @ 10kHz, -172 dBc/Hz @ 100kHz). A third source of error is through the coupling of amplitude noise to phase noise. While the bias was set to suppress amplitude noise, this suppression is far from perfect, on the order of -15dB [3]. Thus, amplitude noise bleed-through is expected to contribute to error.

Given the sources of error in this measurement, the experimental results reasonably illustrate the relationship between both measurement techniques.

Chapter 6

Experiments Measuring Timing Jitter of a Passively Modelocked Fiber Laser Using Frequency Discrimination

In this chapter, experiments which use frequency discriminator techniques to measure timing jitter in a 10MHz fundamentally modelocked P-APM laser are described. The performance of the frequency discriminator system is observed. The timing jitter of the system is calculated, based on the measurements made and their limitations.

6.1 Experimental Setup

6.1.1 Passively Modelocked P-APM Fiber Laser System

Figure 6-1 shows the laser system used. Most of the length of the laser consists of Erbium-Doped Fiber and Dispersion Shifted Fiber (DSF) sections. In these section, nonlinear polarization rotation via the Kerr Effect occurs[1]. This results in higher

[1]Nonlinear polarization rotation due to the Kerr Effect occurs in the Single-Mode Fiber (SMF) fiber also. Most of the length of this laser cavity is made up of the Erbium and DSF sections, and

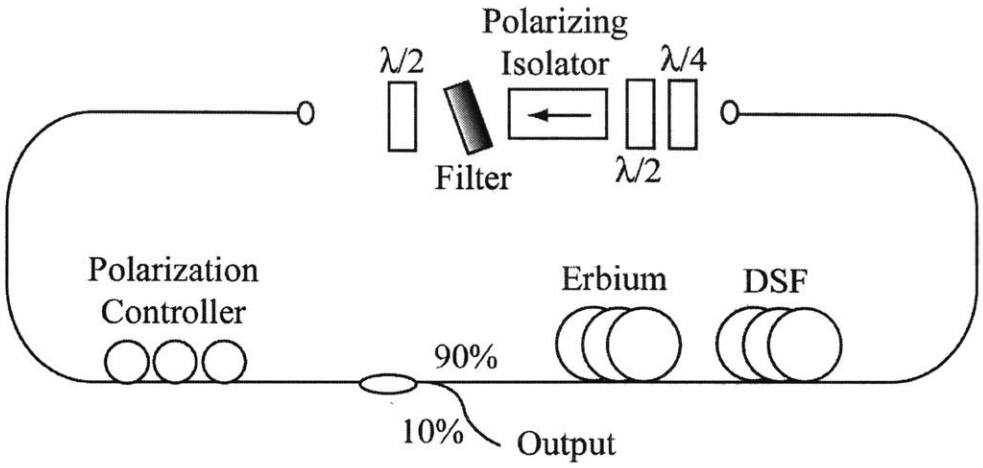

Figure 6-1: The P-APM 10MHz laser.

intensities emerging from the fiber in one state of polarization, and lower intensities in a different polarization state. Subsequently, the polarizing isolator is reached, and different loss is experienced depending on the polarization state, i.e. the intensity. When the waveplates and polarization paddles are properly biased so that higher intensities pass through the polarizing isolator with less loss, modelocked operation is favored [18].

It should be noted that other bias points exist. Very often, near the modelocked bias points there lies a bias point that causes Q-switching. Additionally, there are very stable continuous wave (CW) states, where CW modes of operation are favored, resulting from biasing that suppresses modelocking.

The discrete nature of soliton pulse energies, as shown in Section 4.1 by the Area Theorem, can also be seen in this system. At sufficient pump energies, on the order of 80mW and above, the cavity can support multiple pulses per round trip. How the energy is distributed, i.e. what pulse configurations are over a round-trip period, is fairly random and extremely hysteretic, as seen by oscilloscope traces. The multiple-pulse operation is eliminated by reducing the pump power while in a modelocked state until one pulse per round trip operation (fundamental modelocking) is achieved.

thus we treat nonlinear polarization rotations elsewhere as negligible.

The laser was pumped with an SDL MOPA Laser (Model 5762) at 978nm. The pump beam is coupled into Flexcore fiber and forward pumps the Erbium using a Gould 980/1550 WDM fiber coupler. The typical pump power level that supported single-pulse operation was $35mW \pm 10mW$, depending on the polarization paddle and waveplate settings. In many cases, the laser would fall out of modelocking as the pump power was reduced before single-pulse operation could be reached.

Typical average optical output power from the laser in this state was $150\mu W$ at the 10% output port. The pulse parameter width, τ, of the output pulses was 520fs as shown in Figure 6-3.

A typical optical spectrum is shown in Figure 6-2. One may initially assume that the two lobes on the side are Kelly sidebands [19][20]. However, this may not be the case. The optical filter being used has a 7.5nm bandwidth, and falls off sharply. When CW lasing, the spectrum clearly shows where the edges of the filter lie. Those edges correspond exactly with the dips between the main peak and side peaks of the modelocked spectrum. Thus it seems that the filter causes this feature.

Given the Fourier transform of a square function, one expects this square filter shape to cause lobes to appear in the time domain, on either side of the pulse. (The Fourier transform of a square is a function of the form $\frac{\sin(x)}{x}$.) The auto-correlation of the pulse is shown in Figure 6-3, and indeed, the lobes do appear.

Traces for various ranges over the RF spectrum are given in Figure 6-5. The even distribution of the energy into the harmonics shown in the 0Hz to 2GHz trace gives indication that there is one pulse, not multiple pulses, per round-trip time. The roll off of this plot is due to the bandwidth of the RF amplifiers (0-1GHz) used in detection. The trace from 0Hz to 200MHz shows the uniformity of the harmonic peaks. The final trace is a close-up of the fundamental repetition rate peak, and shows that this frequency is 10.378MHz.

6.1.2 Frequency Discriminator Setup

A frequency discriminator measurement system, shown in Figure 6-6 was constructed to measure the timing jitter. The P-APM laser output was split using a 20%-80%

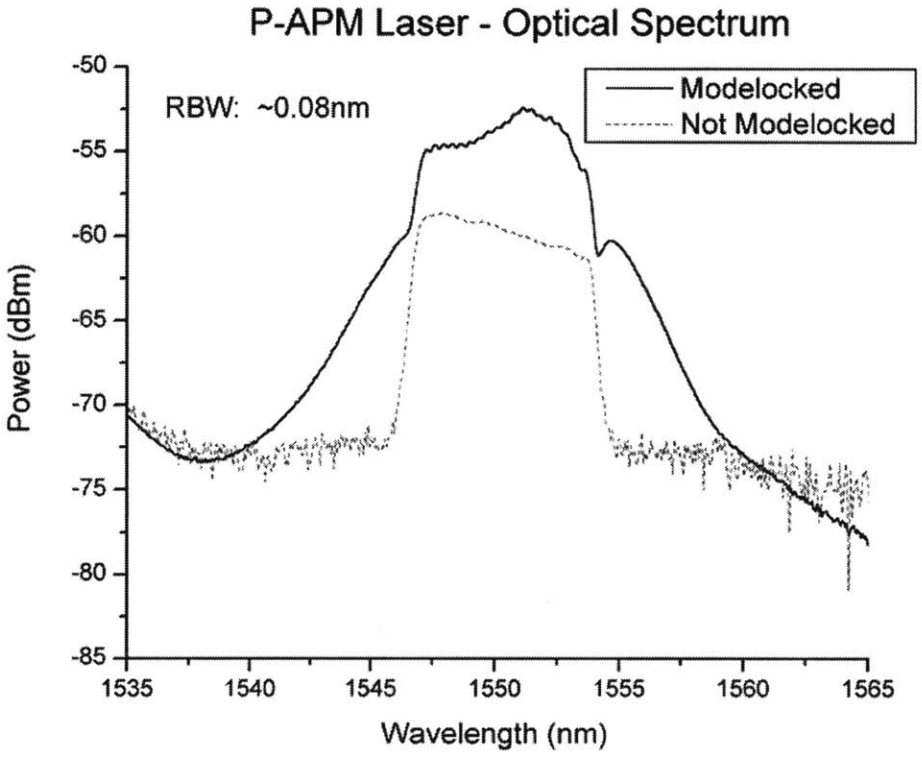

Figure 6-2: Typical modelocked spectrum of the P-APM fiber laser. Overlayed on this is the laser output when not in a modelocked state. One can clearly see the filter edges coinciding with the dips in the modelocked spectrum.

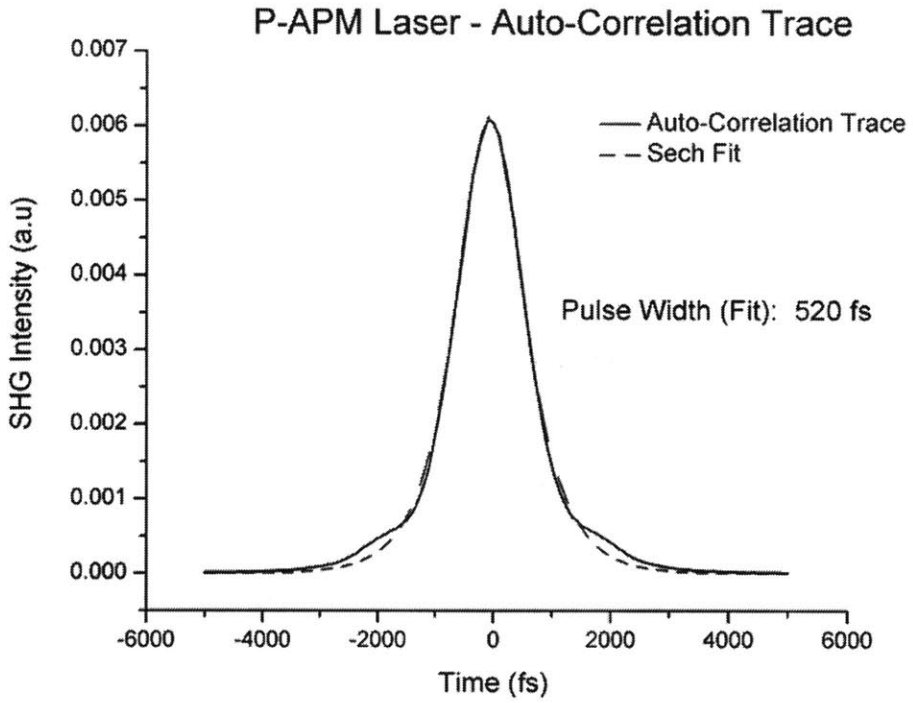

Figure 6-3: Typical auto-correlation of the P-APM fiber laser. A dashed line shows a secant hyperbolic fit to the auto-correlation trace. The bumps in the wings of the pulse are attributed to the optical filter shape.

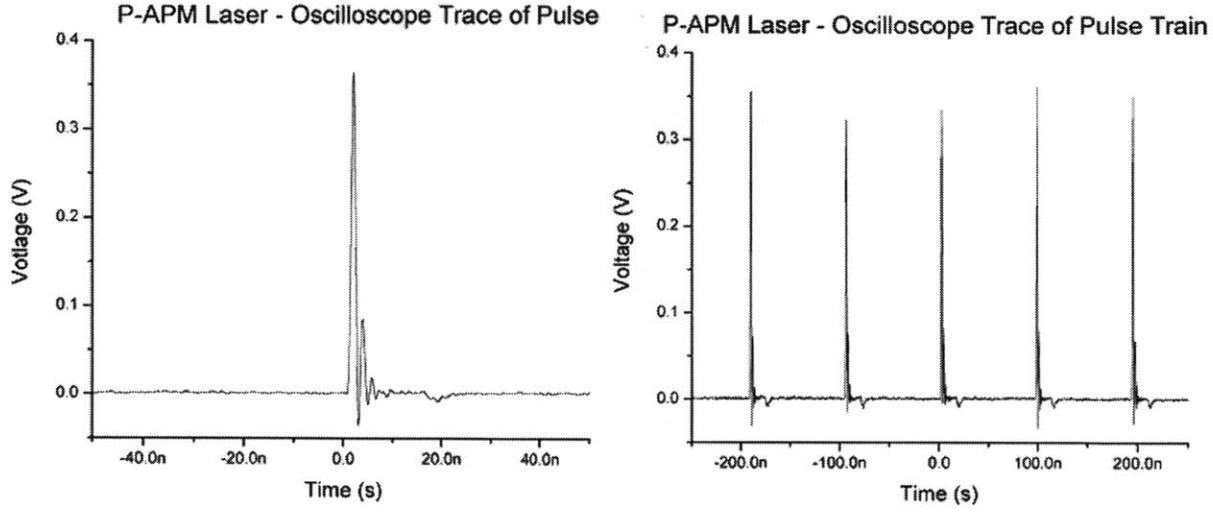

Figure 6-4: Digital Oscilloscope trace of a single optical pulse, and the optical pulse train.

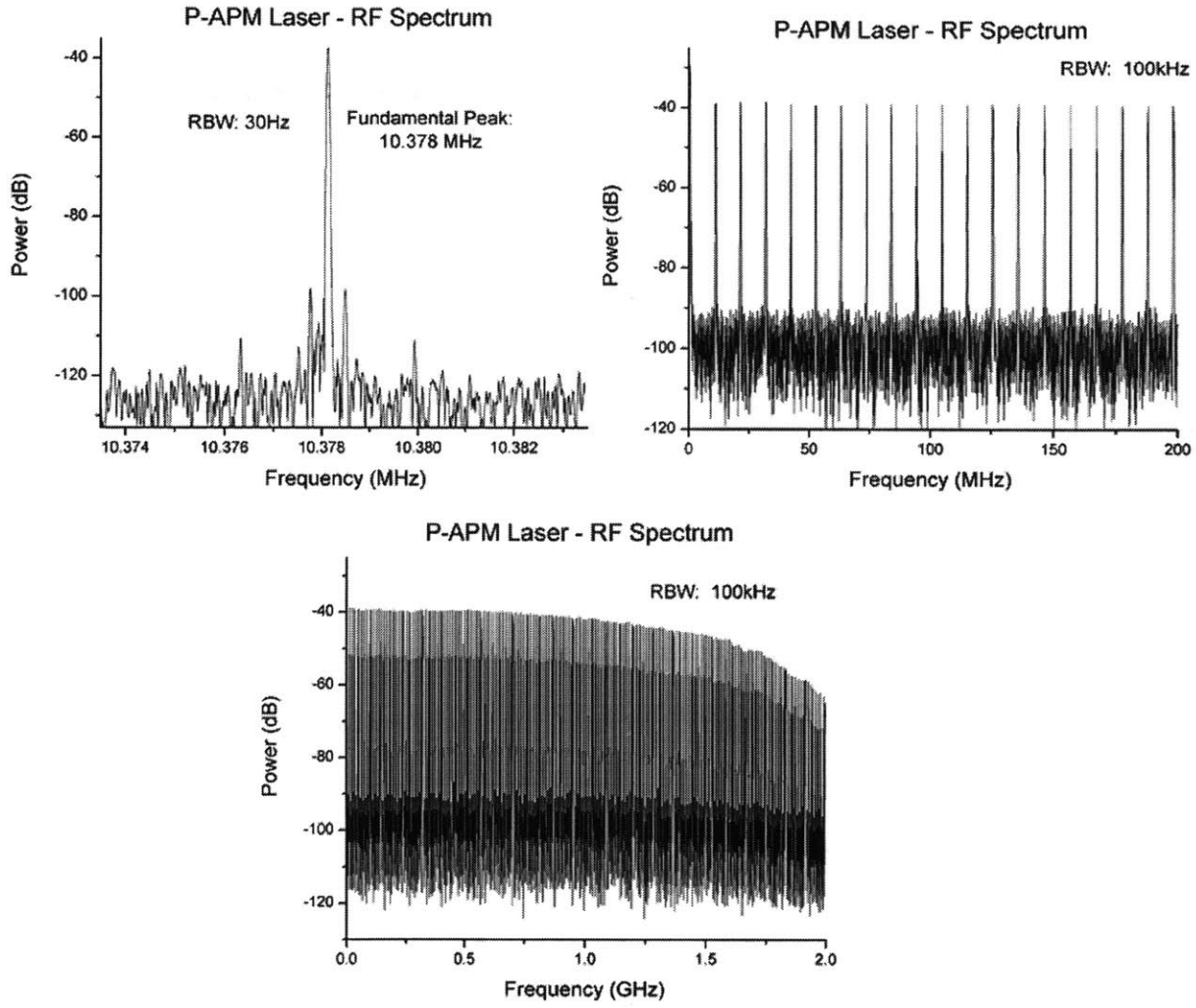

Figure 6-5: Various plots of the RF spectrum of the laser output.

coupler. The 20% path was split again with a 1%/99% coupler, where the 1% port went to the optical spectrum analyzer and the 99% port went to the optical correlator. The 80% port served as the input to the frequency discriminator setup. This port was split with a 50%/50% coupler. One output was fed to the LO detector. The other port is delayed by a changeable fiber delay line, and then fed to the RF detector. Both the RF and LO detector are Discovery Semiconductor DSC40S detectors with a 16GHz bandwidth, chosen to match each other as closely as was possible in their responsivity. The delay lines were made of Corning LEAF fiber, with a dispersion of 5 ps/nm/km.

The detected signals were then filtered by a Mini-Circuits bandpass filter (Model SBP-10.7, 10MHz CWL, 3.7MHz BW), and then by a low-pass filter (Mini-Circuits, Model SLP-750, 750MHz). The resulting signal was then amplified by two cascaded low noise amplifiers (Mini-Circuits, ZFL-1000LN, +20dB gain, NF 2), attenuated to appropriate levels to avoid amplifier compression, amplified by another amplifier (Mini-Circuits, Model ZKL-2, +29dB gain, NF 5), DC blocked (Arra, 1-9572E), phase delayed in the RF arm (two Arra delays, Model 3448B, 2π @ 1GHz range each), and fed into the mixer (Mini-Circuits, Model ZFM-4, Level +7dBm) ports. Immediately before the mixer port, a -20dB tap (Mini-Circuits, Model ZFDC-20-5) was placed to monitor the power into the mixer to ensure optimal mixing. The mixer output was filtered with another low-pass filter (Mini-Circuits, Model SBP-3, 3MHz) leave a DC signal.

6.1.3 Determining K_ϕ

By measuring the spectral noise density of the voltage, one can calculate the timing jitter spectral density. This calculation requires the conversion from voltage noise spectral density to phase noise spectral density, and thus a measurement of the conversion constant, K_ϕ, is needed, as shown in Equation (3.28).

This is done by adjusting the RF path length until an average of zero voltage at the output is seen. This average was viewed using an averaging function on a Tektronix digital oscilloscope (Model: TDS 380, 400MHz BW). Once this zero average voltage

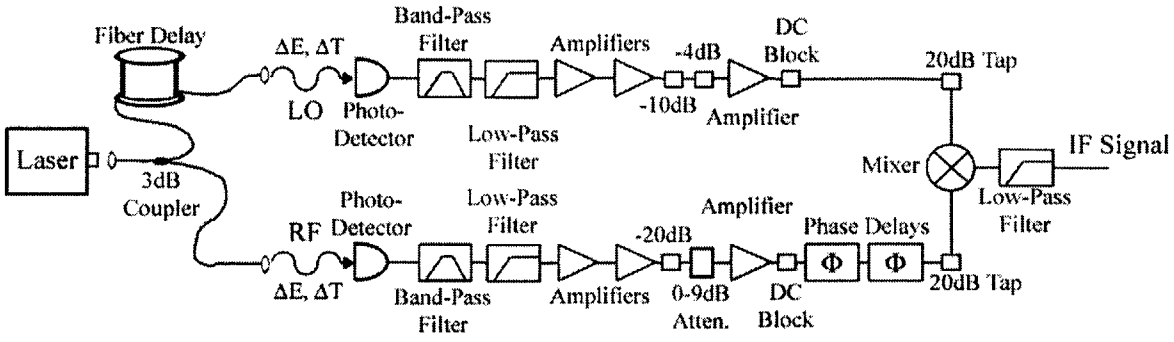

Figure 6-6: The frequency discriminator system used for these measurements.

is found, the RF path length was adjusted small amounts using the phase delay, and the delay amount (in radians) and voltage recorded. The slope of a linear fit to these data points provided the slope of the voltage vs. phase, which is precisely K_ϕ.

This process was performed out before each spectrum is taken. Each set of calibration data consisted of at least four data points.

6.2 Results and Conclusions

Using the frequency discriminator, voltage noise spectral densities were taken for delay lengths of 0m (noise floor), 500m, 1000m, 2000m, 4000m, 5000m, and 6000m. The complete set of data is shown in Section C.1 in terms of the voltage noise spectral density. Figure 6-7 presents two single sideband spectra, assuming no pulse correlation. Because the pulse correlation is not known, single sideband measurements, $\mathcal{L}(f_m)$, can not be plotted with quantitative accuracy, but can provide qualitative information.

6.2.1 Sensitivity

One will immediately notice the oscillations that begin to appear at higher frequencies. In Section 3.3.2, the sensitivity for a frequency discriminator system was derived, concluding that the sensitivity has a $\frac{\sin(x)}{x}$ dependence. The oscillations that appear

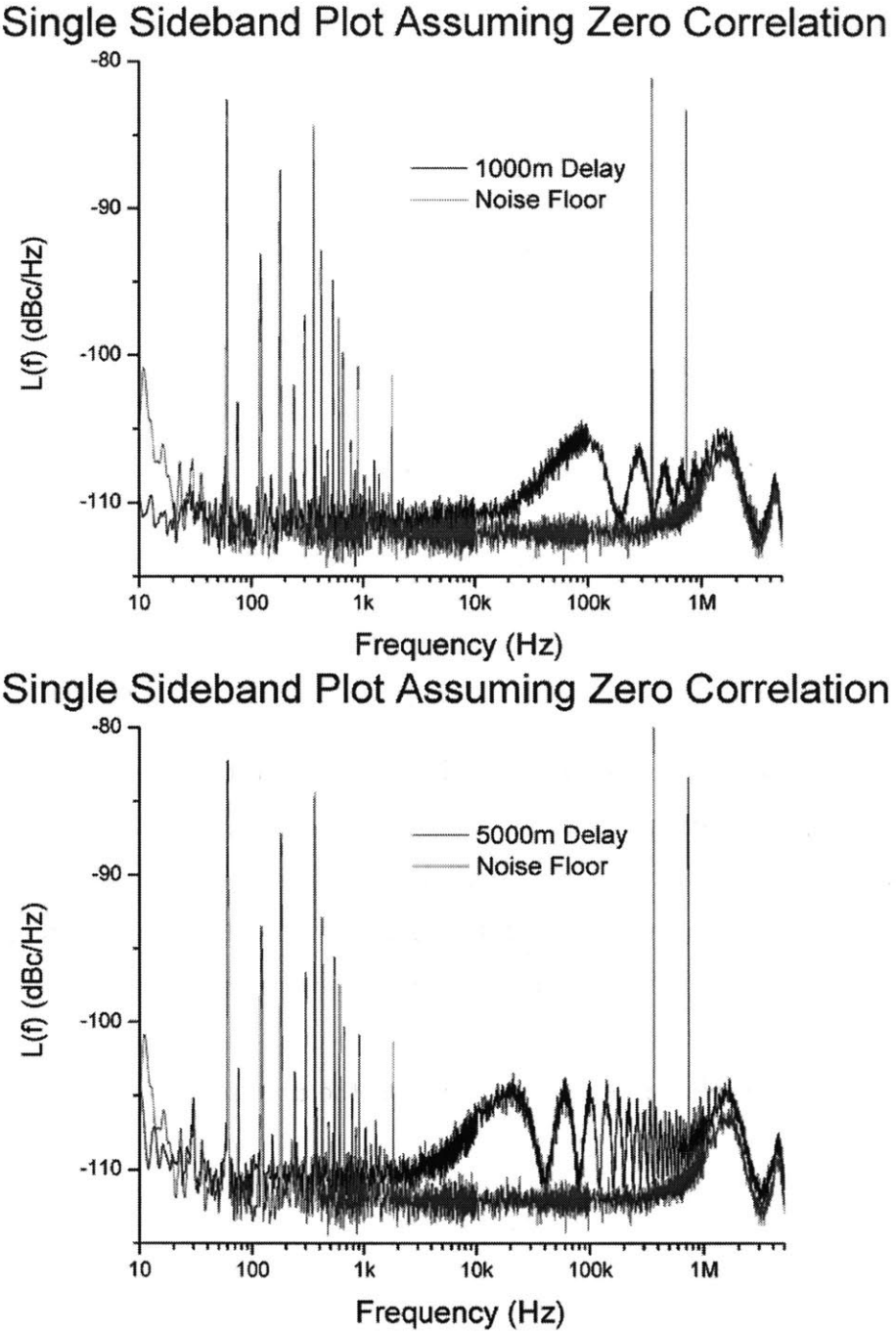

Figure 6-7: Frequency discriminator single sideband plot of timing jitter, assuming no correlation. Delay length is 1000m / 5.0μs (top), and 5000m / 25.0μs (bottom).

in the data match up extremely well with the theoretically predicted sensitivity.

6.2.2 Extracting the Correlation as a Function of Delay

Equation (3.28) shows the correlation function in the expression for the voltage fluctuations. It has been shown in [9] that for a fundamentally modelocked laser, the mean-squared jitter, i.e. the correlation function, should be:

$$\langle \Delta T(0) \Delta T(nT_R) \rangle = \frac{D}{2\gamma T_R}(1-\gamma T_R)^{|n|} \approx \frac{D}{2\gamma T_R} e^{-\gamma T_R |n|} \tag{6.1}$$

where the approximation holds when $\gamma T_R << 1$.

Because this exponential decay of the correlation affects the noise spectral density, an attempt can be made to extract this correlation from the data. One may integrate the timing noise spectral densities for each delay length, and observe the resulting dependence of the timing jitter on delay length. Ideally, this will result in a measurement of γT_R. Considering the $\frac{sin(x)}{x}$ sensitivity limitations of the frequency discriminator measurement, a portion of the spectrum must be chosen where, for every delay length, the system is sensitive enough to take valid data. Figure 6-8 shows the sensitivity plots for the time delays used in this experiment. From this, it is concluded that the frequency range from 175kHz to 191.7kHz is most appropriate.

The resulting calculated RMS timing jitter values over this bandwidth are plotted in Figure 6-9 as a function of delay length. As expected, the integrated timing noise increases as the correlation decreases. However, the expected $1 - e^{Rt}$ dependence is not seen.

The extraction of the correlation coefficient would benefit from careful choice of delay lengths to maximize the overlap range. High-resolution plots of the overlapping frequency band to be integrated would also greatly improve the accuracy.

6.2.3 Timing Jitter Results

Although the noise spectral density results do not allow the extraction of a number for the timing jitter, attempts were made to extract limits for the timing jitter, making

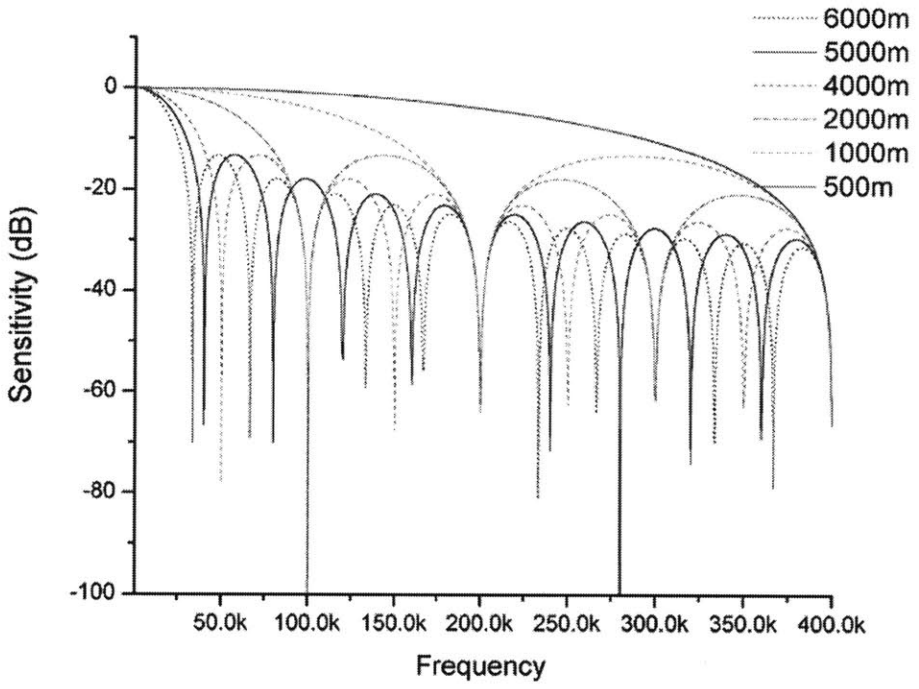

Figure 6-8: Plot of the sensitivity of the frequency discriminator as a function of frequency for various delay lengths. The first null frequency decreases as the delay length is increased.

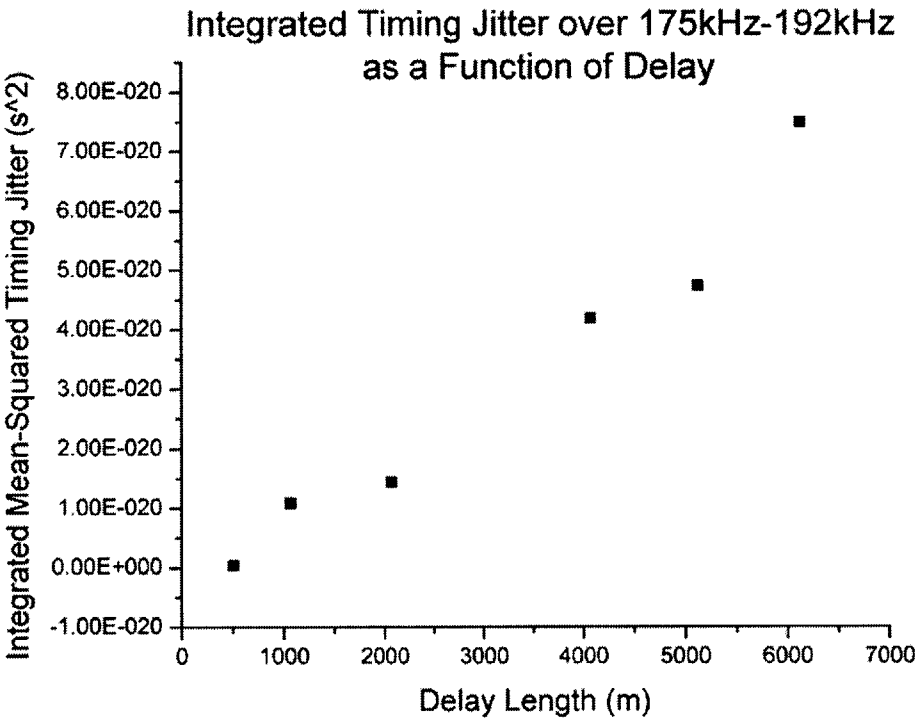

Figure 6-9: Plot of the integration over 175kHz to 191.7kHz of $S_{\Delta T,\Delta T} - S_{\Delta T(0),\Delta T(t_d)}$ data, as a function of delay length.

certain assumptions.

The first calculation made was to plot the timing noise spectral density noise floor, and integrate out to the Nyquist frequency. This result will give some idea of the minimum amount of RMS timing jitter one can measure. Of course, the actual minimum is dependent on the spectral distribution of the timing jitter. Either way, an integral of the noise floor, using Equation (3.5), results in a timing jitter of 168ps.

A similar calculation for the 6000m delay length, executed without $\frac{sinx}{x}$ correction or regard to the noise floor, yields an RMS timing jitter of 248ps.

Given the lack in the data of any spectral characteristics predicted by the theory, as well as many other uncertainties, it is not believed that these numbers are valid.

6.2.4 Conclusions

This set of experiments produced inconclusive results.

It seems that the data is masked by the noise floor at low, rising out at higher frequencies. This seems strange, considering that the frequency discriminator should show maximal sensitivity at low frequencies, and that a passively modelocked laser should exhibit a timing noise spectral density that is greatest at lower frequencies.

Also, it appears that the noise spectrum first "rises out" of the noise floor at increasingly higher frequencies as the delay is lengthened. One would expect that longer delays would increase the sensitivity a lower frequencies and cause the "rising out" frequency to decrease as the delay is lengthened. This leads to the conclusion that data that appears to be above the noise floor, while clearly related to the sensitivity of the frequency discriminator, is not timing jitter in the optical pulse train.

More specifically, it is believed that the spectral densities are dominated by extraneous noise. This conclusion is based on several observations. In attempts leading up to acquiring the data presented, the filters in the frequency discriminator arms were place after the amplifiers. In those preliminary data sets, the sensitivity oscillations in the noise spectral density were not as clearly seen.

The filters were moved before the amplifiers in order to increase the average power at the mixing to necessary levels for the mixer to operate correctly. However, by

moving the filters before the amplifiers, all of the unwanted noise from the amplifiers is now allowed to reach the mixer, and thus the mixing products of the amplifier noise shows up in the data. Additionally, large integrated spectral density numbers were seen. Therefore, it is believed that the timing jitter is below the noise floor. Filtering earlier in the frequency discriminator should improve performance.

The noise floor also seems to show oscillatory behavior in the MHz range. This behavior seems to appear around 2-3MHz, and is attributed to the 3 MHz bandwidth of the 3MHz band-pass filter after the mixer and the 3MHz bandwidth of the 10.7MHz bandpass filters. Obviously, the filters interfere with results at these frequencies. Ideally, filters should be used that flatly pass out to the Nyquist frequency.

If indeed it is laser timing noise that is rising out of the noise floor, the shape of the optical filter may be partly responsible for the disparity between the experimental and theoretical characteristics of the noise spectral density. The filter drops off very quickly, so the expansion of the filter shape to second order in the timing noise spectral density derivation in Section 4.2 may neglect significant higher-order contributions. In Section 5.1.3 it was observed that the filter greatly effecting the timing jitter, so it seems plausible that the filter may play a significant role here.

At this point, the only fundamental limitation of the frequency discriminator seems to be the bandwidth limitations.

6.2.5 Future Work

Several future experiments can be pursued as extensions of this work.

The simplest is to further optimize the current setup. The laser system would benefit greatly from a more appropriate optical filter. Much room for optimization of the frequency discriminator to decrease the noise floor also exists. Although this thesis showed that, theoretically, using laser output harmonics will not improve the system's sensitivity 3.3.2, this should be verified experimentally.

Another question arose during this work: One detects the optical pulse train, and looks at the phase noise as an indication of the optical pulse train noise. When one observes a higher harmonic of the pulse train, how does one interpret the phase noise

at a position in time corresponding to a position between pulses in the optical pulse train? Future work may pursue this and similar questions.

Ultimately, the interesting application of the frequency discriminator is to measure the timing jitter of quiet passively modelocked laser systems. The current P-APM laser, modified for regenerative phase modulation [21] qualifies as one of these systems, and measurements of this laser's noise will be pursued.

Chapter 7

Summary

In this work, optical correlation, residual phase noise, and frequency discriminator techniques for measuring the timing jitter of an optical pulse train were reviewed. Experiments comparing the results of an optical correlation and residual phase noise measurement were compared, and reasonably close results were found.

Soliton perturbation theory was also reviewed, and observed for the case of active and passive modelocking. Experiments using the frequency discriminator technique to measure the timing jitter of a polarization additive-pulse modelocked fiber laser were carried out. The current experimental results allowed for few concrete conclusions; however, there are many avenues left to explore to improve the performance of the system and the results of experiments.

Appendix A

Physical Derivations Reference

A.1 Dispersion

The combined effect of material and waveguide dispersion are important in considering fiber laser operation, and are vital to the existence of solitons. The relationship between two parameters used to express the group velocity dispersion (GVD) of a particular dielectric waveguide is sought here. This section is based on [14].

For a wave with frequency ω travelling down a waveguide there is an associate wavevector, $\beta(\omega)$. We expand β in a Taylor Series about zero frequency in order to express the wavevector's dependence on frequency as a sum of polynomials:

$$\beta(\omega) = \beta(\omega = 0) + \left[\frac{\partial\beta}{\partial\omega}\right]_{\omega=0} \omega + \frac{1}{2}\left[\frac{\partial^2\beta}{\partial\omega^2}\right]_{\omega=0} \omega^2 + ...$$

$$\beta(\omega) = \beta_0 + \beta'\omega + \frac{1}{2}\beta''\omega^2 + ... \tag{A.1}$$

β'' is the GVD, which describes the curvature of the wavevector's dependence on frequency, and is most commonly given in units of ps^2/km.

The D parameter is another expression of the GVD, and is related to β'' in the following way:

$$D = -\frac{2\pi c}{\lambda^2}\beta'' \tag{A.2}$$

D is normally given in units of $ps/nm/km$. Normal dispersion, where longer (red) wavelengths propagate faster than shorter (blue) wavelengths, corresponds to $\beta > 0, D < 0$. Anomalous dispersion, where short (blue) wavelength propagate faster than longer (red) wavelengths, corresponds to $\beta < 0, D > 0$.

Appendix B

Mathematical Review

B.1 Review of Basic Probabilistic Quantities and Concepts

This section is primarily intended as a reference to the reader. Most of the information for this section is taken from [22]. We follow this source's notation, where we write random variables with capitalized variables, and nominal values of that variable with lowercase variables.

B.1.1 Probability Density Function

The Probability Density Function (PDF) describes how likely a particular random variable is to take on a value that falls within a given range. Thus, if we consider random variable X, which has a PDF called $f_X(x)$, then the probability that X will take on a value between x and $x + \delta$ is given by:

$$P(x < X < x + \delta) = \int_x^{x+\delta} dx f_X(x) \tag{B.1}$$

For two random variables, X and Y, we can define the joint PDF, describing how X and Y vary with respect to each other. We write this as $f_{X,Y}(x, y)$. From this, we can find the PDFs of each variable alone, the marginal PDFs. For example, the marginal PDF of X is found as follows:

$$f_X(x) = \int_{-\infty}^{\infty} f_{X,Y}(x,y)dy \tag{B.2}$$

B.1.2 Expectation

The expectation, or first moment, of a random variable describes the mean, or average value that a random variable will take on. The expectation of random variable, X, is written as $E[X]$ or as $\langle X \rangle$.

One can also take expectations of functions of random variables. For a function of continuous random variable, X, the expectation is given as:

$$E[g(X)] = \langle g(X) \rangle = \int_{-\infty}^{\infty} g(x) f_X(x) dx \tag{B.3}$$

For functions of continuous random variables, X and Y, the expectation is given as:

$$E[g(X,Y)] = \langle g(X,Y) \rangle = \int_{-\infty}^{\infty} \int_{-\infty}^{\infty} g(x,y) f_{X,Y}(x,y) dx dy \tag{B.4}$$

B.1.3 Variance and Mean-Squared Value

The variance of a random variable describes how spread out the probability distribution is - how it "varies". The variance of random variable, X, is written as $varX$ and is defined as:

$$var(X) = E[(X - E[X])^2] = E[X^2] - (E[X])^2 = \langle X^2 \rangle - \langle X \rangle^2 \tag{B.5}$$

which we see is a function of the first and second moment. Notice that, when the expectation is zero, the variance equals the mean-squared value, $\langle X^2 \rangle$.

One can take variances of functions of random variables, in an analogous way to that shown in Equation (B.3) and Equation (B.4).

B.1.4 Moments

Generally, one can talk about the moments of a PDF, where the n^{th} moment is given as $E[X^n]$. Knowledge of the value of every moment of a given PDF will uniquely specify the PDF.

B.1.5 Covariance and Correlation Function

As the variance describes how a random variable varies, the covariance describes how two random variables vary relative to each other. The covariance of random variables, X and Y, is given by:

$$cov(X,Y) = E[(X - E[X])(Y - E[Y])] = E[XY] - E[X]E[Y] = \langle XY \rangle - \langle X \rangle \langle Y \rangle \tag{B.6}$$

Notice that when either the expectation of X or Y are zero, the covariance is equal to the correlation function for X and Y, $\langle XY \rangle$.

B.1.6 Correlation Coefficient

The correlation coefficient, $\rho(X,Y)$, is a normalized version of the covariance. $|\rho(X,Y)|$ expresses the degree of correlation and ranges from 0 to 1, and the sign of $\rho(X,Y)$ expresses the sign of the correlation (whether X and Y tend to have the same or opposite signs). The correlation coefficient is given as:

$$\rho(X,Y) = \frac{cov(X,Y)}{\sqrt{var(X)var(Y)}} \tag{B.7}$$

Note that perfect correlation does not imply that the random variables have the same PDFs. Also note that the correlation coefficient and the correlation function are related, but are not the same thing.

B.1.7 Variance of the Sum of Two Random Variables

For the general random variables, X and Y, the variance of their sum is given as:

$$var(X+Y) = var(X) + var(Y) + 2cov(X,Y) \tag{B.8}$$

or in terms of mean-squared values and correlation functions, we see the expectation cancel and find:

$$\langle (X+Y)^2 \rangle = \langle X^2 \rangle + \langle Y^2 \rangle + 2\langle XY \rangle \tag{B.9}$$

B.1.8 Independent Random Variables

Two random variables, X and Y, are said to be independent when the probability distribution of one is not effected by knowledge of the other variable. Independence is formally defined when the joint PDF of X and Y are related to the marginal PDFs of X and Y by the following:

$$f_{X+Y}(x+y) = f_X(x) f_Y(y) \tag{B.10}$$

B.1.9 A Few Consequences of Independence

Independence leads to the following consequences:

1. The $cov(X,Y) = 0$. X and Y are uncorrelated.

2. The PDF of the sum of X and Y, call it Z, is the convolution of the PDF of X and the PDF of Y:

$$f_Z(z) = \int_\infty^\infty f_X(x) f_Y(z-x) = \int_\infty^\infty dy f_Y(y) dx f_X(z-y) \tag{B.11}$$

3. The variance of Z equals the sum of the variances of X and Y:

$$var(X+Y) = var(X) + var(Y) \tag{B.12}$$

and thus:

$$\langle (X+Y)^2 \rangle = \langle X^2 \rangle + \langle Y^2 \rangle \tag{B.13}$$

B.1.10 Central Limit Theorem

The central limit theorem, an expression of the strong law of large numbers, states that the sum of a large number of independent random variables tends to have a distribution that is Gaussian, regardless of the probability distribution of each independent random variable.

B.2 Pulse Width Measures

In this section, we summarize the analytic and numerical relationship between various measures of pulse width.

B.2.1 Definition of Widths

One can indicate the width of a pulse in different ways. Here we classify some of those ways as the pulse width, the full-width half-maximum, and the variance width.

Pulse Width

The definition of pulse width varies from pulse shape to pulse shape. The pulse width is consistently labelled as τ or τ_i.

Full-Width Half-Maximum

The full-width half-maximum takes the usual definition, which is the width of the pulse at one half of its maximum height. For pulse $I_i(t)$, We notate the full-width half-maximum as $FWHM(I_i)$.

Variance Width

The variance width is defined using an analogy with probability calculations. We normalize the pulse shape, and treat it as though it were a PDF for a random variable. We then calculate the variance of that PDF.

Notationally, for pulse $I_i(t)$, we denote the variance width as $varW(I_i)$, where we suppress the unnecessary argument of the function.

Notice that in our notation, the argument of $varW()$ can be written normalized, but we do not require it. In calculating $varW()$, however, we must be sure to take the variance of the normalized argument of the function. Failing to do so will lead to factors, specifically, inverse normalization constants, that we do not want.

B.2.2 Gaussian Widths

For gaussian pulses, we consider the form:

$$f(t) = e^{-\frac{t^2}{2\tau^2}} \tag{B.14}$$

where τ we call the pulse width.

We find that the FWHM scales linearly with the pulse width, as expected, and that the variance scales with the square of the pulse width. We can solve these relationship analytically, and we find:

$$FWHM(f) = 2\sqrt{ln(2)}\left(\sqrt{2}\tau\right) \tag{B.15}$$

$$varW(f) = 2\tau^2 \tag{B.16}$$

B.2.3 Secant Hyperbolic Widths

For secant hyperbolic pulses, we consider the form:

$$f(t) = sech\left(\frac{t}{\tau}\right) \tag{B.17}$$

where τ we call the pulse width.

We find that the FWHM also scales linearly with the pulse width, and that the variance scales with the square of the pulse width. The coefficients resulting from numerical calculations are included in the following equations:

$$FWHM(f) = 2.8000\tau \tag{B.18}$$

$$varW(f) = 2.461\tau^2 \tag{B.19}$$

Appendix C

Data

C.1 Frequency Discriminator Data

In this section, the raw data as taken for the experiments in Chapter 6 is presented. Each plot contains the single sideband voltage noise spectral density for a specific delay, along with the noise floor and theoretical sensitivity curve.

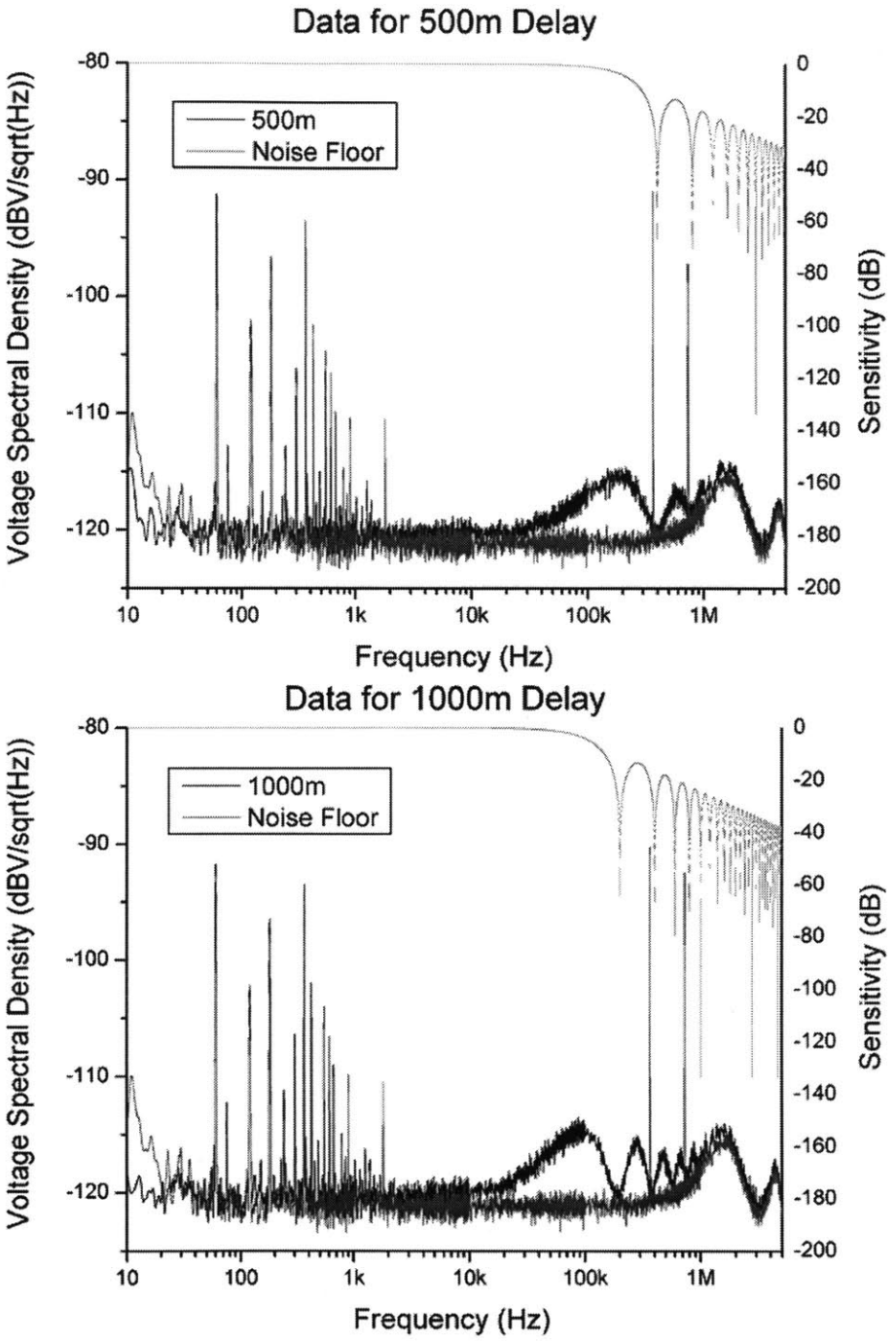

Figure C-1: Voltage noise spectral density and sensitivity plots for 500m ($2.5\mu s$) and 1000m ($5.0\mu s$) delay.

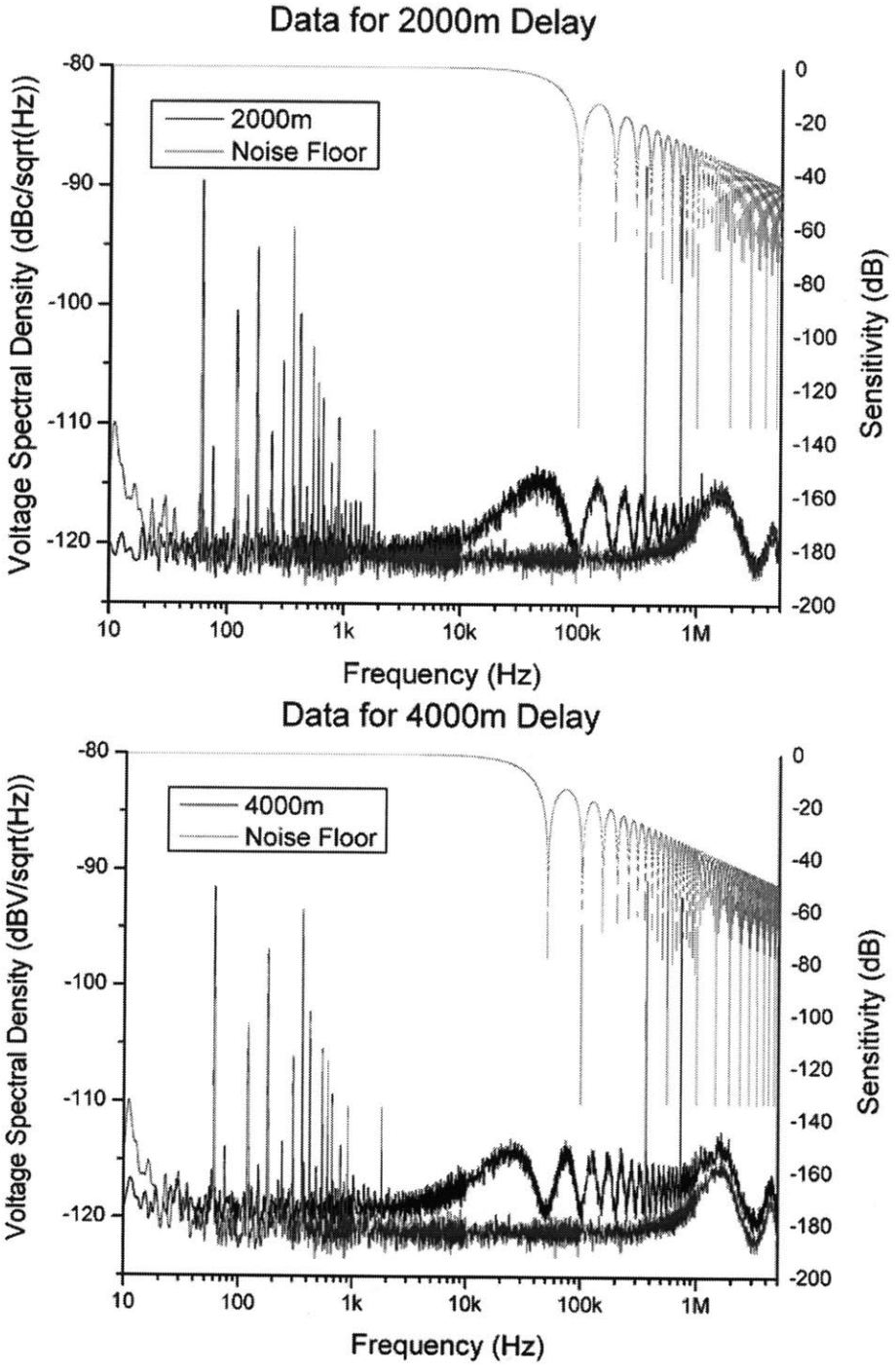

Figure C-2: Voltage noise spectral density and sensitivity plots for 2000m ($10.0\mu s$) and 4000m ($20.0\mu s$) delay.

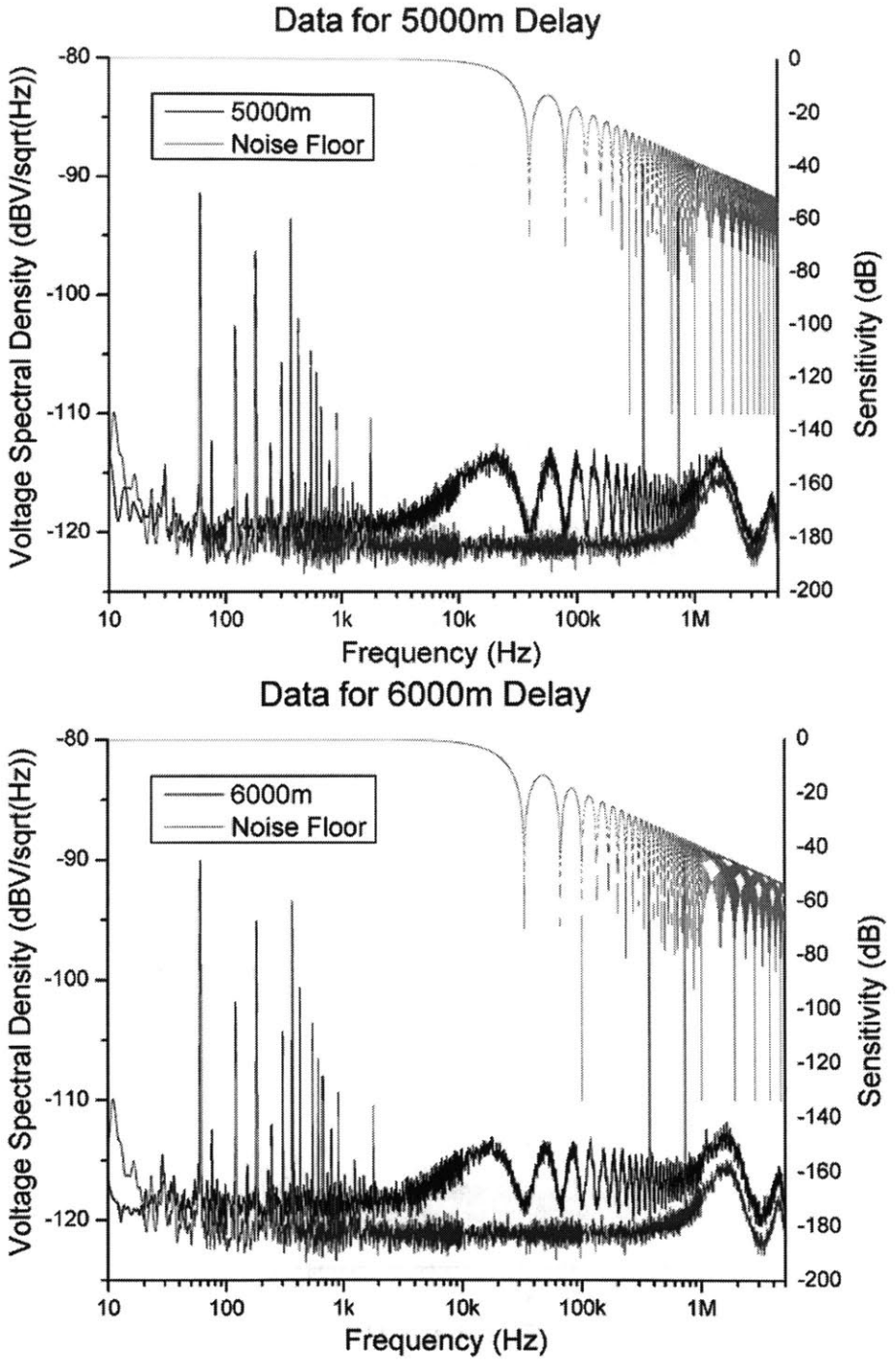

Figure C-3: Voltage noise spectral density and sensitivity plots for 5000m ($25.0\mu s$) and 6000m ($30.0\mu s$) delay.

Bibliography

[1] Paul W. Juodawlkis, Jonathon C. Twichell, Gary E. Betts, Jeffrey J. Hargreaves, Richard D. Younger, Jeffrey L. Wasserman, Fredrick J. O'Donnell, Kevin G. Ray, and Richard C. Williamson. Optically sampled analog-to-digital converters. *IEEE Transactions On Microwave Theory and Techniques*, 49(10):1840–1853, October 2001.

[2] Robert H. Walden. Analog-to-digital converter survey and analysis. *IEEE Journal on Selected Areas in Communcations*, 17(4):539–550, April 1999.

[3] Matthew Edward Grein. *Noise and Stability of Actively Modelocked Fiber Lasers.* PhD dissertation, Massachusetts Institute of Technology, Department of Electrical Engineering and Computer Science, 2002.

[4] Leaf Alden Jiang. *Ultralow-Noise Modelocked Lasers.* PhD dissertation, Massachusetts Institute of Technology, Department of Electrical Engineering and Computer Science, May 2002.

[5] Darpa/eto photonic a/d converter technology (pact) kick-off meeting. MIT-Lincoln Laboratory, Lexington, MA, 1999.

[6] Erich P. Ippen. Principles of passive mode locking. *Applied Physics B: Lasers and Optics*, 58:159–170, 1994.

[7] Leaf Alden Jiang. A comparison of various technologies for optical autocorrelations of picosecond pulses at 1.5μm. Paper written in fulfillment of Area Examination at M.I.T., 2001.

[8] Robert W. Boyd. *Nonlinear Optics.* Academic Press, San Diego, California, first edition, 1992.

[9] Farhan Rana, Harry L. T. Lee, Rajeev J. Ram, Matthew E. Grein, Leaf A. Jiang, Erich P. Ippen, and Hermann A. Haus. Characterization of the noise and correlations in harmonically mode-locked lasers. *Journal of the Optical Society of America*, 19(11):2609–2621, November 2002.

[10] Paul W. Juodawlkis, Jonathon C. Twichell, Jeffrey L. Wasserman, Gary E. Betts, and Richard C. Williamson. Measurement of mode-locked laser timing jitter by use of phase-encoded optical sampling. *Optics Letters*, 26:289–291, 2001.

[11] D. von der Linde. Characterization of the noise in continuously operating mode-locked lasers. *Applied Physics B*, 39:201–217, November 1986.

[12] Ryan P. Scott, Carsten Langrock, and Brian H. Kolner. High-dynamic-range laser amplitude and phase noise measurement techniques. *IEEE Journal On Selected Topics In Quantum Electronics*, 7(4):641–655, July 2001.

[13] Hewlett-Packard. Product note 11729c-2: Phase noise characterization of microwave oscillators. Technical report, Hewlett-Packard, 1985.

[14] Kohichi Robert Tamura. *Additive Pulse Mode-Locked Erbium-Doped Fiber Lasers.* PhD dissertation, Massachusetts Institute of Technology, Department of Electrical Engineering and Computer Science, 1994.

[15] A. Hasagawa and F. Tappert. Transmission of stationary nonlinear optical pulses in dispersive dielectric fibers. *Applied Physics Letters*, 23:142–144, 1973.

[16] Hermann A. Haus and Antonio Mecozzi. Noise of mode-locked lasers. *IEEE Journal of Quantum Electronics*, 29:983–996, 1993.

[17] M. E. Grein, L. A. Jiang, H. A. Haus, E. P. Ippen, C. McNeilage, J. H. Searls, and R. S. Windeler. Observation of quantum-limited timing jitter in an active, harmonically mode-locked fiber laser. *Optics Letters*, 27:957–959, 2002.

[18] M. Hofer, M. E. Fermann, F. Haberl, M. H. Ober, and A. J. Schmidt. Mode lcoking with cross-phase and self-phase modulation. *Optics Letters*, 16:502–504, 1991.

[19] S.M.J. Kelly. Characteristic sideband instability of periodically amplified average soliton. *Electronics Letters*, 28:806–807, 1992.

[20] Michael L. Dennis and Irl N. Duling III. Experimental study of sideband generation in femtosecond fiber lasers. *IEEE Journal of Quantum Electronics*, 30:1469–1477, 1994.

[21] M. Margalit, C. X. Yu, S. Namiki, E. P. Ippen, and H. A. Haus. Harmonic mode-locking using regenerative phase modulation. *IEEE Photonic Technology Letters*, 10:337–339, 1998.

[22] Dimitri P. Bertsekas and John N. Tsitsiklis. *Introduction to Probability.* Pre-first edition, 2002.